

1
2 **NPEPPS regulates intracellular import and sensitivity to cisplatin by**
3 **interaction with volume regulated anion channels**
4

5
6 Robert T. Jones^{1,15}, Andrew Goodspeed^{1,3,15}, Maryam C. Akbarzadeh^{2,4,16}, Mathijs Scholtes^{2,16},
7 Hedvig Vekony¹, Annie Jean¹, Charlene B. Tilton¹, Saswat Mohapatra⁵, Michael V. Orman¹,
8 Stephanie Araki¹, Molishree Joshi^{1,6}, Mahmood Javaid⁷, Eric T. Clambey⁸, Ryan Layer^{7,9},
9 Teemu D. Laajala^{1,10}, Sarah Parker¹¹, Tokameh Mahmoudi^{2,12}, Tahlita Zuiverloon^{2,*},
10 Dan Theodorescu^{5,13,14,*} and James C. Costello^{1,3,17,*}
11

12 ¹Department of Pharmacology, University of Colorado Anschutz Medical Campus, Aurora, CO,
13 USA

14 ² Department of Urology, Erasmus MC Cancer Institute, Erasmus University Medical Center
15 Rotterdam, Rotterdam, The Netherlands

16 ³University of Colorado Comprehensive Cancer Center, University of Colorado Anschutz
17 Medical Campus, Aurora, CO, USA

18 ⁴Stem Cell and Regenerative Medicine Center of Excellence, Tehran University of Medical
19 Sciences, Tehran, Iran

20 ⁵Cedars-Sinai Samuel Oschin Comprehensive Cancer Institute, Los Angeles, CA, USA

21 ⁶Functional Genomics Facility, University of Colorado Anschutz Medical Campus, Aurora, CO,
22 USA

23 ⁷Computer Science Department, University of Colorado, Boulder

24 ⁸Department of Anesthesiology, University of Colorado Anschutz Medical Campus, Aurora, CO

25 ⁹BioFrontiers Institute, University of Colorado, Boulder

26 ¹⁰Department of Mathematics and Statistics, University of Turku, Turku, Finland.

27 ¹¹Smidt Heart Institute & Advanced Clinical Biosystems Research Institute, Cedars Sinai
28 Medical Center, Los Angeles, California 90048, United States

29 ¹²Erasmus MC, Department of Biochemistry, Rotterdam, The Netherlands

30 ¹³Department of Surgery, Cedars-Sinai Medical Center, Los Angeles, CA, USA

31 ¹⁴Department of Pathology and Laboratory Medicine, Cedars-Sinai Medical Center, Los
32 Angeles, CA, USA

33 ¹⁵Equal first authors

34 ¹⁶These authors contributed equally

35 ¹⁷Lead Contact

36 *Corresponding Authors
37

38 **Corresponding Authors**
39

40 Tahlita Zuiverloon, MD, PhD

41 Department of Urology

42 Erasmus MC Cancer Institute, Erasmus University Medical Center

43 Dr. Molewaterplein 40

44 3015GD, Rotterdam

45 The Netherlands

46 +31 6 26 41 90 87

47 t.zuiverloon@erasmusmc.nl
48

49 Dan Theodorescu, MD, PhD
50 Departments of Surgery and Pathology
51 Cedars-Sinai Medical Center
52 8700 Beverly Blvd.
53 OCC Mezz C2002
54 6/19/21 11:26:00 PMLos Angeles, CA 90048
55 +1 (310) 423-8431
56 dan.theodorescu@cshs.org

57
58 James C Costello, PhD
59 Department of Pharmacology
60 University of Colorado Anschutz Medical Campus
61 Mail Stop 8303
62 12801 E. 17th Ave., Rm L18-6114
63 Aurora, CO 80045
64 +1 (303) 724-8619
65 james.costello@cuanschutz.edu

66 67 **HIGHLIGHTS**

- 68
- 69 • Multi-omic screening found NPEPPS is a driver of cisplatin resistance in cancer
- 70 • NPEPPS is in protein complex with LRRC8A and D, volume regulated anion channel
- 71 (VRAC) subunits
- 72 • LRRC8A and D loss increases cisplatin resistance and reduce its intracellular levels
- 73 • NPEPPS regulates cisplatin import and sensitivity through VRACs
- 74 • NPEPPS function is inhibited by small molecules offering potential for clinical translation

75 76 **KEY WORDS**

77
78 NPEPPS; Volume Regulated Anion Channel; CRISPR Screen; Synthetic Lethality; multi-omics;
79 Bladder Cancer; DNA Repair; Cisplatin; Tosedostat

80 **ABSTRACT**

81

82 Despite routine use of platinum-based chemotherapeutics in cancer treatment, there remains a
83 need to improve efficacy and patient selection. Multi-omic assessment of human bladder cancer
84 cell lines and their cisplatin resistant derivatives and whole-genome CRISPR screens identified
85 NPEPPS, the puromycin-sensitive aminopeptidase as a novel driver of cisplatin resistance.
86 NPEPPS depletion increased cisplatin import and sensitization of resistant cells *in vitro* and *in*
87 *vivo*. Pharmacologic inhibition of NPEPPS in cells and chemoresistant, patient-derived tumor
88 organoids improved response to cisplatin. NPEPPS was found in complex with volume
89 regulated anion channel (VRAC) subunits LRRC8A and LRRC8D, whose loss is known to
90 enhance resistance to cisplatin. Depletion of LRRC8A the only obligate subunit for normal
91 VRAC function abrogated the effect of NPEPPS-mediated cisplatin import. Our findings
92 describe the first mechanism by which VRACs can be targeted for therapeutic benefit.

93 INTRODUCTION

94

95 Platinum-based chemotherapeutics have a long history (Dilruba and Kalayda, 2016; Rottenberg
96 et al., 2021) with successful applications in testicular, ovarian, bladder, head and neck, and lung
97 cancers. However, these drugs come with dose-dependent side effects that limit patient
98 eligibility. Additionally, chemoresistance mechanisms can arise, reducing the efficacy of these
99 drugs. While mechanisms of resistance have long been established, including DNA damage
100 repair and drug export (Galluzzi et al., 2012), other mechanisms, such as the import of platinum
101 drugs through volume regulated anion channels (VRACs) are more recently discovered and
102 present new opportunities for therapeutic development (Planells-Cases et al., 2015; Rottenberg
103 et al., 2021). Despite their limitations, platinum-based drugs remain the standard of care in
104 many cancer types and with a paucity of better treatment options for many patients, these drugs
105 will remain in use for the foreseeable future. Two avenues can improve patient outcomes, which
106 include discovery of more effective agents or development of strategies that can improve
107 efficacy of platinum-based regimens. The latter would have broad impact across a range of
108 cancer types. Here we take the latter approach and focus our efforts on bladder cancer.

109

110 Bladder cancer (BCa) accounts for 430,000 new diagnoses and 170,000 deaths worldwide
111 annually (Bray et al., 2018). Cisplatin-based combination chemotherapy, in the form of
112 gemcitabine plus cisplatin (GemCis) or Methotrexate, Vinblastine, Adriamycin, and Cisplatin
113 (MVAC), remains the first-line, standard of care for metastatic BCa, providing a 5-10% cure rate.
114 However, up to 30% of patients are ineligible for cisplatin-based treatment (Galsky et al., 2018)
115 and are offered carboplatin-based combinations. Unfortunately carboplatin combination therapy
116 has been shown to be less effective in BCa (Patel et al., 2020). Alternatively, immune
117 checkpoint therapies (ICT) are being considered as a first-line therapy (Galsky et al., 2020);
118 however, ICT requires a PD-L1 diagnostic test, for which only ~25% patients meet eligibility
119 (Nadal and Bellmunt, 2019). On top of limited patient eligibility, the complete response rates for
120 ICT eligible patients is 20-30% (Balar et al., 2017), which limits the overall efficacy of ICT across
121 the population of patients with metastatic BCa. Cisplatin-based combination chemotherapy is
122 also standard of care in the neoadjuvant (NAC) setting for the management of localized muscle-
123 invasive bladder cancer (Grossman et al., 2003; Vale, 2005). However, NAC adoption has been
124 slow due to the toxicity of the drugs, the number of patients that are cisplatin ineligible, and the
125 relatively small survival benefit of 5-15% over immediate cystectomy (Witjes et al., 2020).
126 Importantly, in both the metastatic and NAC BCa settings, patient selection and therapeutic
127 efficacy of cisplatin-based chemotherapy remain critical unresolved challenges (Patel et al.,
128 2020).

129

130 Recently, several large-scale efforts have performed whole genome loss-of-function screening
131 across hundreds of cancer cell lines using CRISPR- and shRNA-based libraries to define pan-
132 cancer and context-specific genetic dependencies (Cowley et al., 2014; McDonald et al., 2017;
133 Tsherniak et al., 2017; Behan et al., 2019). A limitation of these efforts is that cells were grown
134 under basal growth conditions in the absence of treatment. Additionally, those studies were
135 performed in cell lines that had not acquired resistance to the treatment. To better understand
136 the functional drivers of therapeutic resistance, such screens must be done in the presence and
137 absence of the therapy of interest (Goodspeed et al., 2019; Huang et al., 2020; Jost and
138 Weissman, 2018; Olivieri et al., 2020), and in cells that have acquired resistance to the
139 treatment itself. Results from such synthetic lethal screens can be used to prioritize gene
140 candidates that can be targeted to overcome treatment resistance.

141

142 In this study, we harnessed the power of CRISPR-based synthetic lethal screening and multi-
143 omic profiling to systematically assess the functional determinants of sensitivity to the treatment

144 regimen of gemcitabine plus cisplatin in a panel of chemoresistant BCa cell lines (**Figure 1A**). In
145 addition to known mechanisms, we present the finding that upregulation of puromycin-sensitive
146 aminopeptidase, NPEPPS, is a novel mechanism of gemcitabine plus cisplatin resistance,
147 specifically affecting cisplatin sensitivity. We provide validation of these findings *in vitro* and *in*
148 *vivo*. We next show that pharmacological inhibition of NPEPPS through an orally deliverable,
149 well-tolerated drug, tosedostat, re-sensitizes resistant cells to cisplatin treatment in BCa cell
150 lines and organoids derived from patient tumors that did not respond to cisplatin-based
151 chemotherapy. We also show that NPEPPS is in complex with VRACs in cancer cells and
152 functionally interacts with VRACs to control the import of cisplatin. These findings describe the
153 first mechanism by which VRAC function can be targeted for therapeutic benefit. We finally
154 provide a unique resource to the community, an R Shiny app for broad comparisons between
155 datasets (CRISPR screens and multi-omic) and cell lines, along with individual gene queries
156 and basic plotting functionality (https://bioinformatics.cuanschutz.edu/BLCA_GC_Omics/).

157 RESULTS

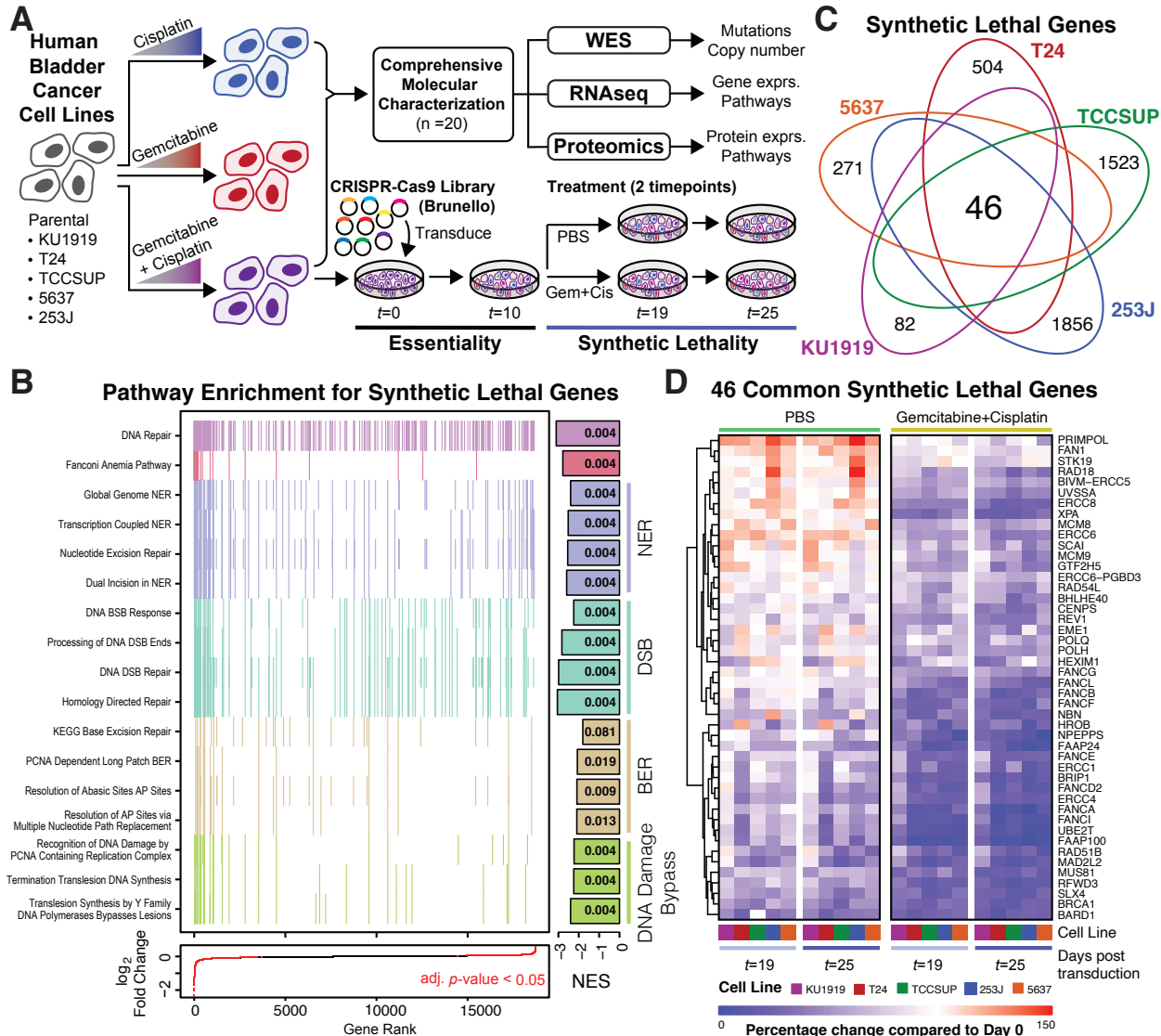
158
159 From the Resistant Cancer Cell Line (RCCL) collection (Vallo et al., 2015, 2017), we obtained
160 five human BCa cell lines, KU1919, 5637, T24, TCCSUP, and 253J. For each, we obtained the
161 parental lines (-Par) and their matched derivatives that were made resistant through dose
162 escalation to cisplatin (-Cis), gemcitabine (-Gem), and the combination of gemcitabine plus
163 cisplatin (-GemCis) (**Figure 1A; Table S1**). We confirmed resistance to the associated drugs for
164 all resistant derivatives in comparison to the parental lines and found them to be consistent with
165 those reported by the RCCL (**Figure S1**) (Vallo et al., 2015, 2017). These cells represent
166 features and alterations in putative BCa drivers as reported in TCGA (Robertson et al., 2017)
167 and variants reported in ClinVar (Landrum et al., 2018) (**Tables 1, S2 and S3**).
168

169 Genome-wide CRISPR screens identify 46 common synthetic lethal genes

170
171 To study the connection between drug resistance and gene expression, we performed whole-
172 genome loss-of-function screens in each of the five GemCis-resistant cell line derivatives. After
173 transduction of the Brunello CRISPR-Cas9 knockout library (Doench et al., 2016), we passaged
174 the cells for 10 days to clear essential genes, then split into saline (PBS) or gemcitabine plus
175 cisplatin treatment groups (**Figure 1A**). Each screen was performed at a drug concentration that
176 allowed the GemCis-resistant cells to grow unrestricted, but which significantly inhibited the
177 growth of the associated parental lines (**Table S1**). Screening parameters for each cell line are
178 reported in **Table S4**. We measured sgRNAs 19 and 25 days after transduction, which were 9
179 and 15 days after the start of treatment.
180

181 We defined genes as “synthetic lethal” with gemcitabine plus cisplatin treatment as those for
182 which the combined cognate sgRNA counts were significantly lower (moderated t-test, FDR <
183 0.05) in the gemcitabine plus cisplatin-treated arm compared to the PBS arm when including
184 both days 19 and 25 in the statistical model (**Table S5**). We identified 235 synthetic lethal genes
185 that were significant in KU1919-GemCis, 888 for T24-GemCis, 2099 for TCCSUP-GemCis,
186 2369 for 253J-GemCis, and 511 for 5637-GemCis. Next, we performed gene set enrichment
187 analysis (Korotkevich et al., 2019) on the full ranked list of genes according to their synthetic
188 lethality. For this analysis, we created one ranked gene list by including each of the five cell
189 types in the statistical model directly. As expected, we found that the top ranked pathways were
190 dominated by processes such as DNA repair, Fanconi Anemia, nucleotide excision repair,
191 double-stranded break repair, base-excision repair, and DNA damage bypass mechanisms
192 (**Figure 1B and Table S6**). These results are consistent with the known roles of DNA damage
193 detection and repair in cisplatin resistance (Drayton and Catto, 2012; Galluzzi et al., 2012).
194

195 Next, we sought to identify the most robust and commonly synthetic lethal candidate genes by
196 identifying only those significant in all 5 cell lines (**Figures 1C and S2**). Of the 46 commonly
197 synthetic lethal genes, and illustrated in **Figure 1D**, some increased cell growth in PBS
198 treatment, then reduced growth in gemcitabine plus cisplatin treatment. Other genes had very
199 little impact on cell growth in PBS treatment, but then reduced growth when treated with
200 gemcitabine plus cisplatin. Finally, some genes reduced cell growth in PBS treatment and
201 further reduced growth with gemcitabine plus cisplatin treatment. As expected, nearly all 46
202 common synthetic lethal candidate genes fell into DNA damage response and repair pathways.



203
204
205
206
207
208
209
210
211
212
213
214

Figure 1. Project overview and synthetic lethal screen results. (A) Human bladder cancer cell lines were made resistant to cisplatin, gemcitabine, or gemcitabine plus cisplatin through dose escalation. All cell lines were profiled using -omic technologies. The gemcitabine plus cisplatin resistant cells were subjected to a pooled CRISPR screen to identify synthetic lethal gene-to-drug relationships. (B) Aggregate gene set enrichment results for the synthetic lethal screen results across all cell lines reveal DNA damage response and repair pathways. Each tick mark represents a gene in the associated pathway. The bars are normalized enrichment scores (NES) with the FDR corrected p-values reported in the bars. (C) When results from all cell lines were evaluated individually, a total of 46 commonly synthetic lethal genes were identified; all counts are reported in Figure S2. (D) The percentage change in the aggregate of the sgRNAs targeting the 46 commonly synthetic lethal genes are reported across saline (PBS) or gemcitabine plus cisplatin treatment arms of the CRISPR screen.

215

Feature	KU1919	T24	TCCSUP	5637	253J
Sex	Male	Female	Female	Male	Male
Stage	T3	Ta	N/A	N/A	T4
Grade	G3	G3	G4	G2	G4
Base47 Subtype	N/A	Basal	Basal	Luminal	Basal
TP53		Y126X	E349X		
HRAS		G12V			
NRAS	Q61R				
PIK3CA			E545K		E545G
TERT					
ARID1A	Y1052X				
KMT2D	T2441Pfs*44			Q2813X	
KDM6A	Q915X				
FAT1		S2682X	D1536N		
KMT2C		R4225X; A3559T			
ERBB2				S310F	
ERBB3		E1219K			
EP300		C1201Y			
FBXW7			S66X		
ASXL2			E330Q		
ATM				H1876Q	
AKT1	E17K				
RYR2		R2401H			
NFE2L2					G81S
RB1			LOSS	Y325X	
E2F3			AMP	AMP	
PPARG				AMP	
CCND1	AMP				
CDKN2A	LOSS				LOSS

216 **Table 1.** Clinicopathologic characteristics and genetic drivers for five cell lines.

217 **NPEPPS is a novel determinant of response to cisplatin**

218

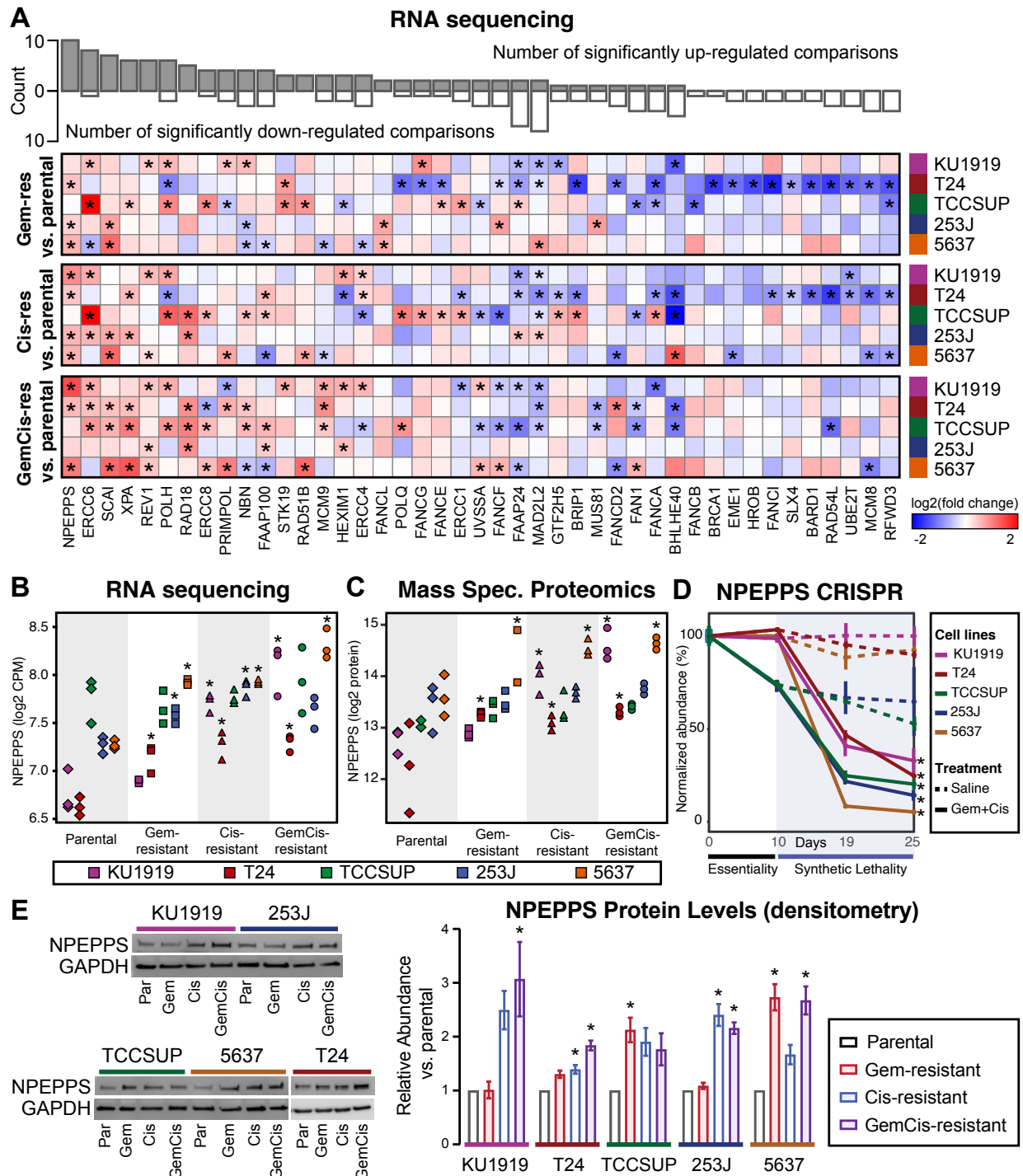
219 A recent systematic analysis of hundreds of CRISPR screens in cancer cell lines with
220 comprehensive multi-omic profiling demonstrated that transcript expression markers were the
221 best predictors of gene dependency (Dempster et al., 2020), providing rationale for the use of
222 pre-treatment -omic profiling as a means to study the biological impact of synthetic lethal hits.
223 Hence, to prioritize the 46 common synthetic lethal genes for validation and detailed
224 mechanistic understanding, we performed RNA sequencing and mass spectrometry-based
225 proteomic profiling on cell lysates of all cell lines grown in drug-free media (**Figure 1A**).

226

227 We investigated the transcriptome and proteome data by comparing parental to matched drug
228 resistant derivative lines (-Gem, -Cis, and -GemCis) and identified several known mechanisms
229 of chemoresistance. For example, acquired resistance to gemcitabine follows a number of
230 common pathways across multiple tumor types that disrupt intracellular metabolism, such as the
231 loss of deoxycytidine kinase (DCK) or increased expression of ribonucleotide reductase subunit
232 M1 (RRM1) (Bepler et al., 2006; Bergman et al., 2005; Jordheim et al., 2011) (**Figure S3A**). Our
233 data shows that RRM1 is specifically and significantly upregulated in nearly all Gem- and
234 GemCis-resistant derivatives in the T24, TCCSUP, KU1919, and 5637 cell line series by both
235 RNA and protein expression. In addition, and with the TCCSUP-GemCis line being the only
236 exception, we found RRM1 copy number amplified, but not in the parental or the cisplatin
237 resistant cells, providing strong support that a robust and consistently acquired mechanism of
238 gemcitabine resistance in these cells is the copy number amplification and subsequent
239 upregulation of RRM1 (**Figure S3B**). RRM1 is defined as an essential gene in the Dependency
240 Map (Tsherniak et al., 2017), which we also detected in our screen (**Table S7**). Interestingly, in
241 253J-Gem and 253J-GemCis cell lines, which had minor changes in RRM1 expression, DCK
242 expression was lost at the RNA and protein level with these results being supported by a copy
243 number loss specific to these cells (**Figure S3B**).

244

245 Next, we analyzed gene and protein expression together while treating the cell line as a
246 covariate in the statistical model. We found 1557 significantly upregulated genes across the
247 Gem-resistant lines, 1897 in the Cis-resistant lines, and 1530 in the GemCis-resistant lines
248 (moderated t-test, FDR < 0.05; **Table S8**). The proteomics data revealed 9 significantly
249 upregulated proteins across the Gem-resistant cell lines, 1 in the Cis-resistant cell lines, and 10
250 in the GemCis-resistant cell lines (moderated t-test, FDR < 0.25; **Table S9**). Given the lower
251 number of significant proteins and the relevance of transcript expression in predicting genetic
252 dependency (Dempster et al., 2020), we first investigated the overlap between the CRISPR
253 screen results and the transcriptomes from each of the resistant cell line derivatives compared
254 to the parental cells. Few genes were significantly and consistently upregulated across the
255 resistant derivatives in the list of 46 commonly synthetic lethal genes (**Figure 2A**), but the most
256 significantly and consistently upregulated genes were involved in DNA damage response and
257 repair mechanisms, including ERCC6, XPA, REV1, POLH, ERRC8, PRIMPOL, NBN, and
258 members of the Fanconi Anemia pathway. Puromycin-sensitive aminopeptidase, NPEPPS, was
259 identified as being the most consistently upregulated gene across the resistant derivatives
260 (**Figure 2A, B**). We similarly found protein levels to be consistently and significantly upregulated
261 (**Figure 2C**). NPEPPS was also a top synthetic lethal hit (**Figure 2D and Table S5**). Consistent
262 with the proteomics results, immunoblotting for NPEPPS revealed that it was upregulated in the
263 Cis-resistant and GemCis-resistant lines, with the Gem-resistant lines showing variable
264 upregulation (**Figure 2E**).

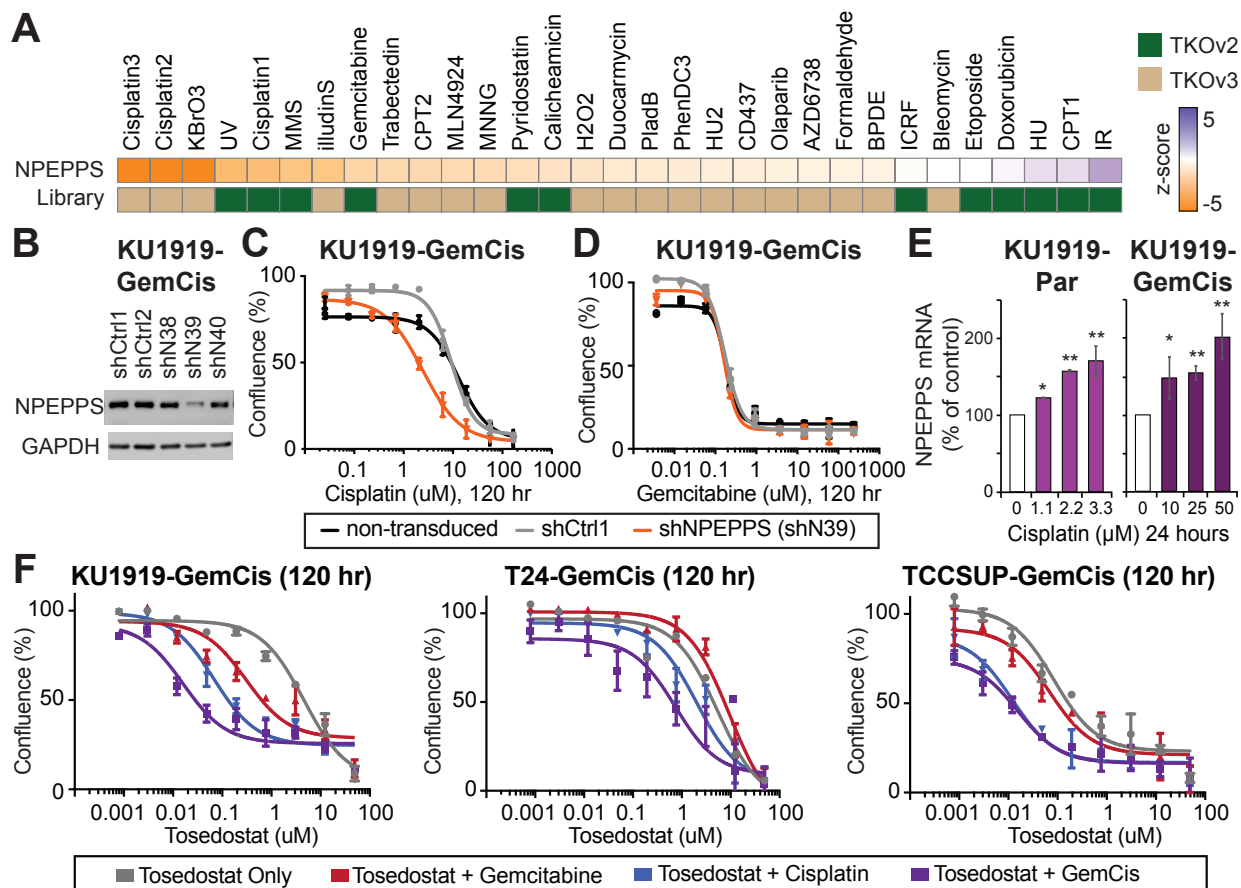


265 **Figure 2. NPEPPS is identified as a commonly upregulated and synthetic lethal hit.** (A) Differential
 266 gene expression of the 46 common synthetic lethal genes as measured by RNaseq across all cell lines,
 267 comparing the treatment resistant derivative (Gem-, Cis-, GemCis-resistant) to the associated parental
 268 cell line. Asterisks indicate a statistically significant result (moderated t-test, *FDR < 0.05). The bar plot on
 269 top is the aggregate count of significant results across all 15 comparisons. Genes are ranked by the count
 270 of statistically significant upregulated hits. (B) RNAseq (compared to parentals; *FDR < 0.05), (C) mass
 271 spectrometry proteomics (compared to parentals, *FDR < 0.25), and (D) CRISPR screen results for
 272 NPEPPS (*FDR < 0.05). (E) Representative immunoblots and densitometry quantification for independent
 273 triplicates (mean ± SEM) for NPEPPS in all cell lines (*FDR < 0.05).

274 We examined an independent whole-genome CRISPR screen that tested 27 general genotoxic
275 agents (Olivieri et al., 2020) and here report new findings in support of NPEPPS as a novel
276 mediator of cisplatin resistance. We found that cells with NPEPPS loss were specifically
277 depleted in response to cisplatin, but not gemcitabine (**Figure 3A**). This result strongly supports
278 the robustness of our findings as Olivieri et al. used different CRISPR libraries (TKOv2 and
279 TKOv3) and cell line (retinal pigment epithelium-1, RPE1). Moreover, our screen results for all
280 five cell lines were highly correlated with the three cisplatin screens (**Figure S4A**). Strikingly,
281 nearly all 46 hits were significant hits associated with cisplatin, but not gemcitabine in Olivieri et
282 al. (**Figure S4B**).

283
284 To validate our finding that NPEPPS depletion enhances sensitivity to gemcitabine plus cisplatin
285 treatment in GemCis-resistant BCa cells, and to parse its role in both cisplatin and gemcitabine
286 resistance, we generated stable NPEPPS shRNA knockdowns in the KU1919-GemCis cell line
287 (**Figure 3B**). The KU1919-GemCis line was selected for further experiments throughout this
288 work because it had the strongest combination of a synthetic lethal result and gene/protein
289 upregulation (**Figure 2**). We found that NPEPPS knockdown preferentially increased cisplatin,
290 but not gemcitabine sensitivity (**Figure 3C, D**). The same result was found using siRNA in the
291 KU1919-GemCis cell line and shRNA and/or siRNA in T24-GemCis and 253J-GemCis cells
292 (**Figure S5**). We also found NPEPPS mRNA increased with cisplatin treatment in both KU1919-
293 Par and KU1919-GemCis cells after 24 hours of treatment (**Figure 3E**). These results indicate
294 that NPEPPS mediates sensitivity to gemcitabine plus cisplatin primarily by its effect on
295 resistance to cisplatin.

296
297 Several agents inhibit NPEPPS activity (Drinkwater et al., 2017). Tosedostat, an orally available
298 M1 aminopeptidase prodrug has antileukemic activity with a favorable toxicity profile in patients
299 (CHR-2797, CAS 238750-77-1) (Cortes et al., 2013; van Herpen et al., 2010; Krige et al., 2008;
300 Löwenberg et al., 2010; Mawad et al., 2016). We tested the response of all GemCis-resistant
301 cells to serial doses of tosedostat at the resistant doses of gemcitabine, cisplatin, and
302 gemcitabine plus cisplatin (**Figure S6**); the KU1919-GemCis, T24-GemCis, and TCCSUP-
303 GemCis cells showed the strongest effects (**Figure 3F**). Consistent with NPEPPS depletion,
304 tosedostat showed minor to no effects in combination with gemcitabine. The strongest
305 combined effect was seen with cisplatin and gemcitabine plus tosedostat treatment (**Figures 3F**
306 and **S6**). These results demonstrate that GemCis-resistant BCa cells can be re-sensitized to
307 cisplatin treatments to varying degrees by genetic and pharmacologic inhibition of NPEPPS.



308
 309 **Figure 3. Genetic and pharmacological inhibition of NPEPPS resensitizes GemCis-resistant cells.**
 310 (A) NPEPPS was found to be synthetic lethal with cisplatin in a CRISPR screen for 27 genotoxic agents
 311 in RPE1 cells by (Olivieri et al., 2020). (B) Immunoblot for NPEPPS across several control and shRNAs
 312 targeting NPEPPS. (C, D) KU1919-GemCis cells with knockdown of NPEPPS treated with increasing
 313 doses of cisplatin or gemcitabine. A total of 3 technical replicates per dose (mean \pm SEM). Independent
 314 experiments are reported in **Figure S5**. (E) NPEPPS mRNA is upregulated in response to cisplatin
 315 treatment in a dose dependent manner in both KU1919-Par and KU1919-GemCis cells. Independent
 316 triplicate experiments are shown (mean \pm SEM) (t-test compared to 0 μ M; *p < 0.05, **p < 0.05). (F)
 317 Pharmacologic targeting of NPEPPS with tosedostat in GemCis-resistant cells treated with cisplatin,
 318 gemcitabine, or gemcitabine plus cisplatin. A total of 3 technical replicates per dose are shown (mean \pm
 319 SEM). Independent experiments are reported in **Figure S6**.

320

321 **Volume regulated anion channels impact chemoresistance in bladder cancer cells**

322

323 NPEPPS is one of 13, M1 aminopeptidases that cleaves amino acids from the N-terminus of
324 polypeptides. NPEPPS is involved in cell growth, development and antigen presentation
325 (Constam et al., 1995; Menzies et al., 2010; Saric et al., 2004; Towne et al., 2008). A role for
326 NPEPPS in chemotherapeutic response is newly described here. To begin characterizing the
327 mechanisms NPEPPS uses to drive cisplatin resistance, we investigated NPEPPS protein
328 interaction partners in the BioPlex interactome, a database that has collected affinity-purification
329 mass spectrometry measurements of systematically over-expressed, tagged proteins (Huttlin et
330 al., 2020). Remarkably, among the small number of proteins that were observed to interact with
331 NPEPPS, were all five subunits of the volume regulated anion channel (VRAC), leucine rich
332 repeat containing 8 VRAC subunit A-E (LRRC8A-E) (**Figure 4A**). Supporting this finding, other
333 affinity-purification mass spectrometry experiments independently reported the interaction
334 between NPEPPS and VRAC members across different cell lines (Kasuya et al., 2018; Syeda et
335 al., 2016). Equally interesting was that none of the other 12, M1 aminopeptidases were found in
336 complex with any VRAC members in the BioPlex interactome. Additionally, none of the other 12,
337 M1 aminopeptidases were found to be synthetic lethal in our CRISPR screens (**Table S5**). To
338 examine if the NPEPPS-VRAC interaction was present in bladder cancer cell lines, we
339 generated FLAG-tagged NPEPPS overexpressing KU1919 and T24 cells. We
340 immunoprecipitated against FLAG and performed immunoblotting against NPEPPS, LRRC8A,
341 and LRRC8D. We found that LRRC8A, the obligate channel member (Qiu et al., 2014), and
342 LRRC8D, which has been previously shown to regulate cisplatin import (Planells-Cases et al.,
343 2015), reliably co-immunoprecipitated with NPEPPS in both cell lines (**Figure 4B**).

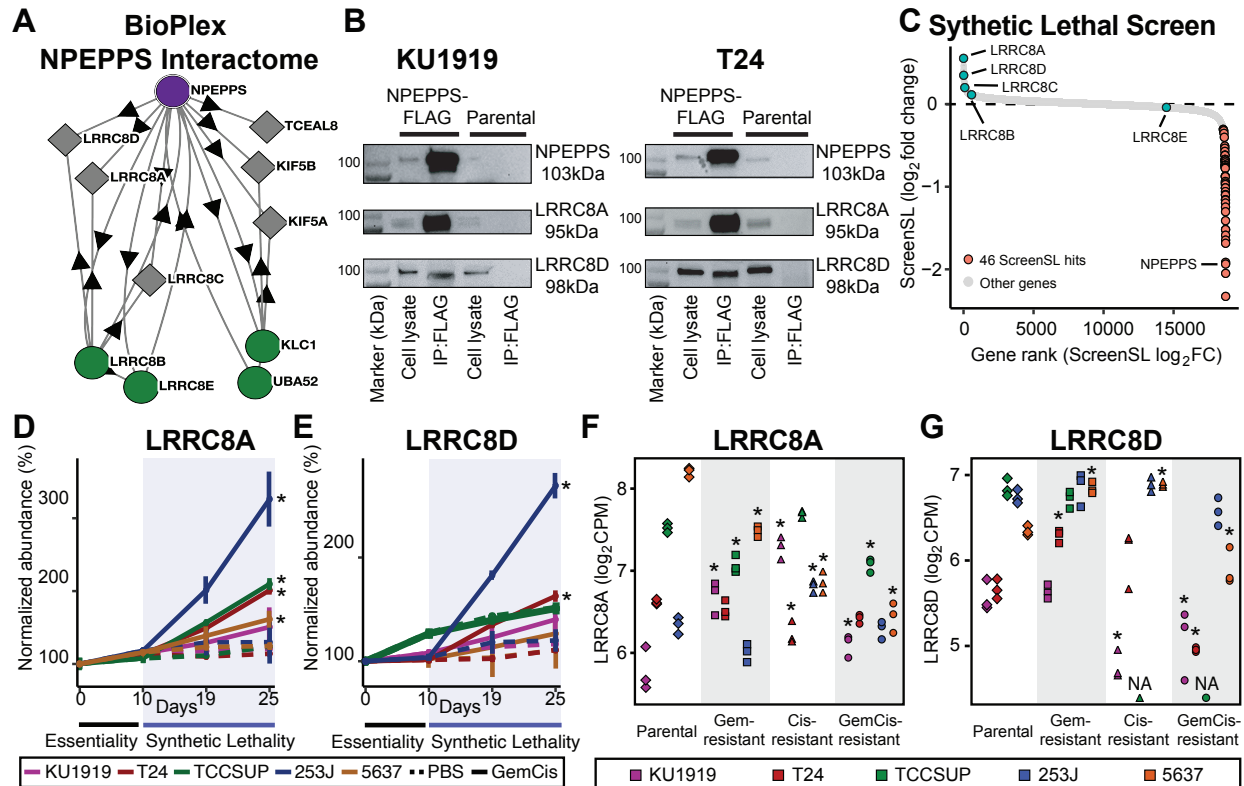
344

345 VRACs directly respond to osmotic stress by trafficking osmolytes such as chlorine, potassium,
346 and taurine, across the plasma membrane to regulate cell volume (Voss et al., 2014).
347 Importantly, the VRAC channel is a hetero-hexamer of subunits that requires the presence of
348 LRRC8A (SWELL1 (Qiu et al., 2014)) to function normally. This is particularly relevant since
349 LRRC8A and LRRC8D are mediators of platinum drug resistance in chronic myelogenous
350 leukemia cells. Knockout experiments in kidney and colorectal cell lines showed that 50-70% of
351 intracellular cisplatin is transported through these channels in isotonic conditions (Planells-
352 Cases et al., 2015), mediated by LRRC8A and LRRC8D. Similar findings were subsequently
353 found in ovarian cancer and alveolar carcinoma cell lines (Sørensen et al., 2014, 2016a,
354 2016b). Thus, we focused on the LRRC8A and LRRC8D subunits for further analysis.

355

356 We revisited our CRISPR screens and RNAseq data to determine if loss of LRRC8A and/or
357 LRRC8D impacted cisplatin resistance. Strikingly, LRRC8A was the 1st and LRRC8D was the
358 11th ranked gene that when lost provided a growth advantage in gemcitabine plus cisplatin
359 treatment across all cell lines (**Figure 4C**). Individually, LRRC8A and LRRC8D loss provide a
360 growth advantage to cells treated with gemcitabine plus cisplatin (**Figure 4D,E**). LRRC8A
361 and/or LRRC8D mRNA expression was reduced for most of the Cis- or GemCis-resistant cell
362 lines, with the Gem-resistant lines showing variable differential expression (**Figure 4F,G**). Most
363 notable, LRRC8D gene expression in the TCCSUP-Cis and TCCSUP-GemCis cells was
364 completely lost (**Figure 4G**). We found that in these cell lines, there is a deep deletion at the
365 LRRC8D locus (**Figure S7**). NPEPPS loss in the TCCSUP-GemCis lines showed the weakest
366 synthetic lethal result compared to the other four GemCis-resistant lines (**Figure 2D**) and
367 LRRC8D loss had no effect on TCCSUP-GemCis growth (**Figure 4E**), while LRRC8A loss did in
368 fact increase growth (**Figure 4D**). Taken together, these data support a functional dependency
369 between NPEPPS and VRAC subunits LRRC8A and LRRC8D in relation to cisplatin resistance.

370



371 **Figure 4. NPEPPS interacts with volume regulated anion channel (VRAC) subunits LRRC8A and**
 372 **LRRC8D to mediate cisplatin response.** (A) NPEPPS is found to interact with all VRAC subunits,
 373 LRRC8A-E, as reported in the BioPlex interactome (Huttlin et al., 2020). (B) Anti-FLAG was used against
 374 KU1919 and T24 parental cell lines as controls and overexpressing FLAG tagged NPEPPS, KU1919 and
 375 T24 cells. The immunoprecipitant was immunoblotted for NPEPPS, LRRC8A, and LRRC8D,
 376 demonstrating that LRRC8A and LRRC8D are pulled down in complex with NPEPPS. (C) Genes ranked
 377 based on \log_2 fold change from the synthetic lethal CRISPR screens across all cell lines. LRRC8A-E and
 378 the 46 common synthetic lethal genes are labeled. (D, E) Knockout of LRRC8A and LRRC8D through the
 379 CRISPR screen resulted in increased cell growth upon gemcitabine plus cisplatin treatment in GemCis-
 380 resistant cell lines (moderated t-test; *FDR < 0.05). (F, G) LRRC8A and LRRC8D gene expression
 381 measured by RNAseq (compared to parentals; *FDR < 0.05).
 382

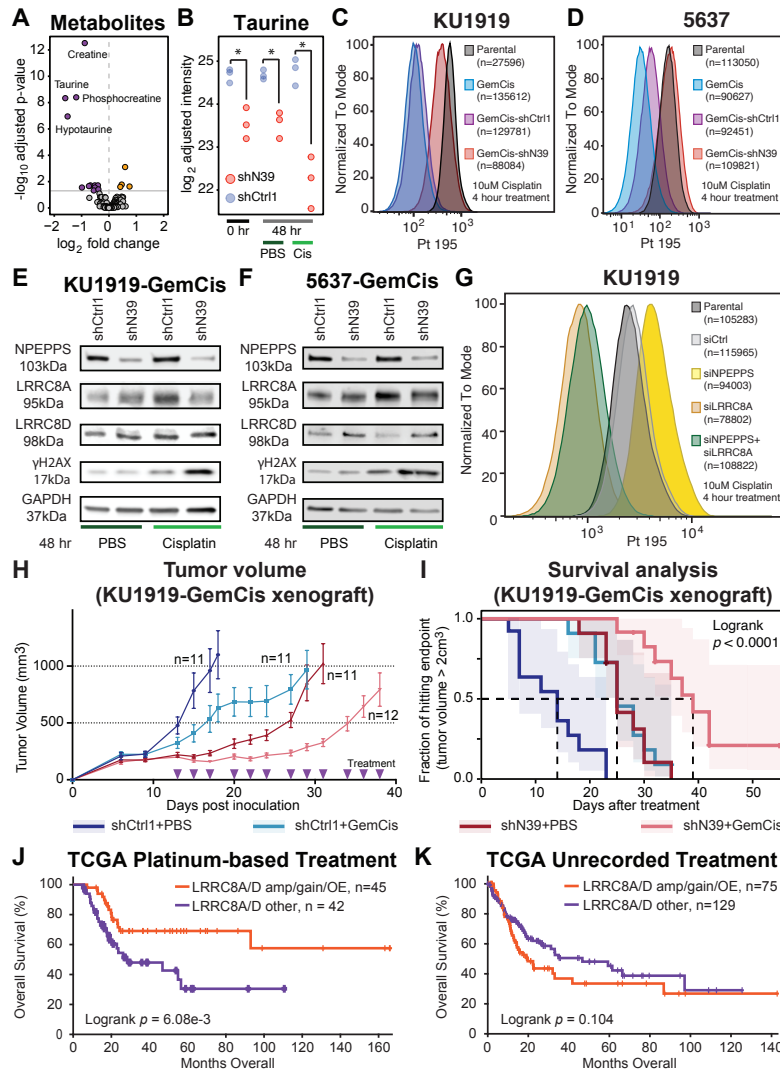
383 Given that VRACs transport cisplatin and carboplatin (Planells-Cases et al., 2015) and finding
384 NPEPPS in complex with LRRC8A and LRRC8D across many cell types (**Figure 4B**) (Huttlin et
385 al., 2020; Kasuya et al., 2018; Syeda et al., 2016), we hypothesized that NPEPPS may be a
386 negative regulator of VRAC activity, consequently reducing import of intracellular cisplatin.
387 Thus, we tested the impact of NPEPPS on osmolytes known to be transported through VRACs.
388 NPEPPS knockdown in KU1919-GemCis-shN39 cells resulted in significantly lower levels of
389 intracellular taurine, hypotaurine, creatine, phosphocreatine, and several other amino acids
390 (**Figure 5A** and **Table S10**), which are known to be exported via VRACs (Jackson and Strange,
391 1993; Planells-Cases et al., 2015; Voss et al., 2014). In addition, intracellular levels of taurine
392 were reduced even further when cells with knockdown of NPEPPS were also treated with 10 μ M
393 cisplatin (**Figure 5B**). This suggests that cisplatin further stimulates channel activity when
394 NPEPPS is decreased, which allows for increased export of taurine, and as we show next,
395 increases cisplatin import.

396
397 To evaluate NPEPPS impact on cisplatin import, we directly measured intracellular cisplatin
398 using the metal ion detection capabilities of cytometry by time-of-flight, CyTOF (Chang et al.,
399 2015). Intracellular cisplatin was measured after 4 hours of treatment at 10 μ M for KU1919-Par,
400 KU1919-GemCis, KU1919-GemCis-shCtrl1, and KU1919-GemCis-shN39 cells. As expected,
401 KU1919-GemCis cells (median Pt 195 = 102) showed decreased uptake of cisplatin compared
402 to KU1919-Par cells (median Pt 195 = 565). Control knockdown had little effect (median Pt 195
403 = 121), but NPEPPS knockdown shifted the intracellular levels of cisplatin to that of parent lines
404 (median Pt 195 = 375), suggesting that NPEPPS depletion allows for increased import of
405 cisplatin (**Figure 5C** and **S8A,B**). These findings were repeated in the 5637 cell lines with highly
406 similar results (**Figure 5D** and **S8C,D**).

407
408 Furthermore, we measured protein levels of LRRC8A and LRRC8D after 48 hours of PBS or
409 10 μ M cisplatin treatment in NPEPPS knockdown or nontargeting control KU1919-GemCis and
410 5637-GemCis cells. Supporting the CyTOF results (**Figure 5C,D**) and the result that taurine is
411 exported at a higher rate upon cisplatin stimulation in the KU1919-GemCis-shN39 cells (**Figure**
412 **5B**), NPEPPS knockdown increased DNA damage as measured by increased γ H2AX foci
413 (**Figure 5E,F** and **S8E,F**). However, we did not find major changes in LRRC8A or LRRC8D
414 expression in response to NPEPPS knockdown or cisplatin treatment (**Figure 5E,F** and **S8E,F**).

415
416 To determine the functional relationship between expression of NPEPPS and VRACs on
417 intracellular cisplatin import, we performed a series of siRNA experiments targeting NPEPPS
418 and/or LRRC8A (**Figure S9A**), the obligate subunit for normal VRAC function as mentioned
419 above (Qiu et al., 2014; Voss et al., 2014). We found that knockdown of NPEPPS in KU1919
420 parental cells increased import of cisplatin (KU1919 median Pt 195 = 1081; KU1919-siNPEPPS
421 median Pt 195 = 1715) (**Figure 5G** and **S9B**); this finding is consistent with our findings in the
422 GemCis-resistant cells (**Figure 5C,D**). As expected, knockdown of LRRC8A resulted in
423 decreased intracellular cisplatin (median Pt 195 = 428), but knockdown of NPEPPS in
424 combination with LRRC8A showed minimal additional effect (median Pt 195 = 498) (**Figure 5G**
425 **and S9B**). These data support a model where NPEPPS mediates cisplatin sensitivity by
426 regulating its intracellular levels through interaction with VRACs.

427



428
429
430
431
432
433
434
435
436
437
438
439
440
441
442
443
444
445
446
447
448
449

Figure 5. NPEPPS regulates VRAC activity and tumor growth in vivo, while LRRC8A/D is predictive of platinum-based treatment response in patients. (A) Volcano plot of metabolites measured from KU1919-GemCis cells with or without NPEPPS knockdown (shN39). Time and treatment (cisplatin 10 μ M) were covariates in the linear model to calculate differential expression using a moderated t-test; horizontal grey line is $-\log_{10}(\text{FDR} = 0.05)$. (B) Taurine abundance measured in KU1919-GemCis cells with non-targeting shRNA controls or shRNA targeting NPEPPS (shN39). Cells were also measured at 48 hours treated with 10 μ M cisplatin or PBS. (C) Intracellular cisplatin levels in (C) KU1919 or (D) 5637 cells were measured after 4 hours of 10 μ M cisplatin treatment using CyTOF, with the number of cells analyzed as indicated. Immunoblot of LRRC8A, LRRC8D, and γ H2AX in (E) KU1919-GemCis-shCtrl1 and KU1919-GemCis-shN39 or (F) 5637-GemCis-shCtrl1 and 5637-GemCis-shN39 cells treated with PBS or 10 μ M cisplatin for 48 hours. (G) Intracellular cisplatin concentrations were measured for KU1919 parental and then for untargeted knockdown (siCtrl) and targeted knockdown of NPEPPS (siNPEPPS), LRRC8A (siLRRC8A), and the combination of NPEPPS and LRRC8A (siNPEPPS+siLRRC8A). (H) Tumor volume of KU1919-GemCis xenografts measured over time and across 4 treatment groups considering non-targeting shRNA controls (shCtrl1), shRNA targeting NPEPPS (shN39), PBS vehicle control (PBS), or gemcitabine plus cisplatin treatment (GemCis). (I) Survival analysis of xenograft models with a defined endpoint of a tumor volume > 2cm³. Logrank test was applied to test significance. (J) Survival analysis of muscle-invasive bladder cancer in the TCGA stratified based on copy number amplification, gain or overexpression of LRRC8A or LRRC8D. Patients all had a record of cisplatin-based chemotherapy treatment. (K) Survival analysis for patients stratified by LRRC8A or LRRC8D as in (J), but that did not have any record of cisplatin-based treatments.

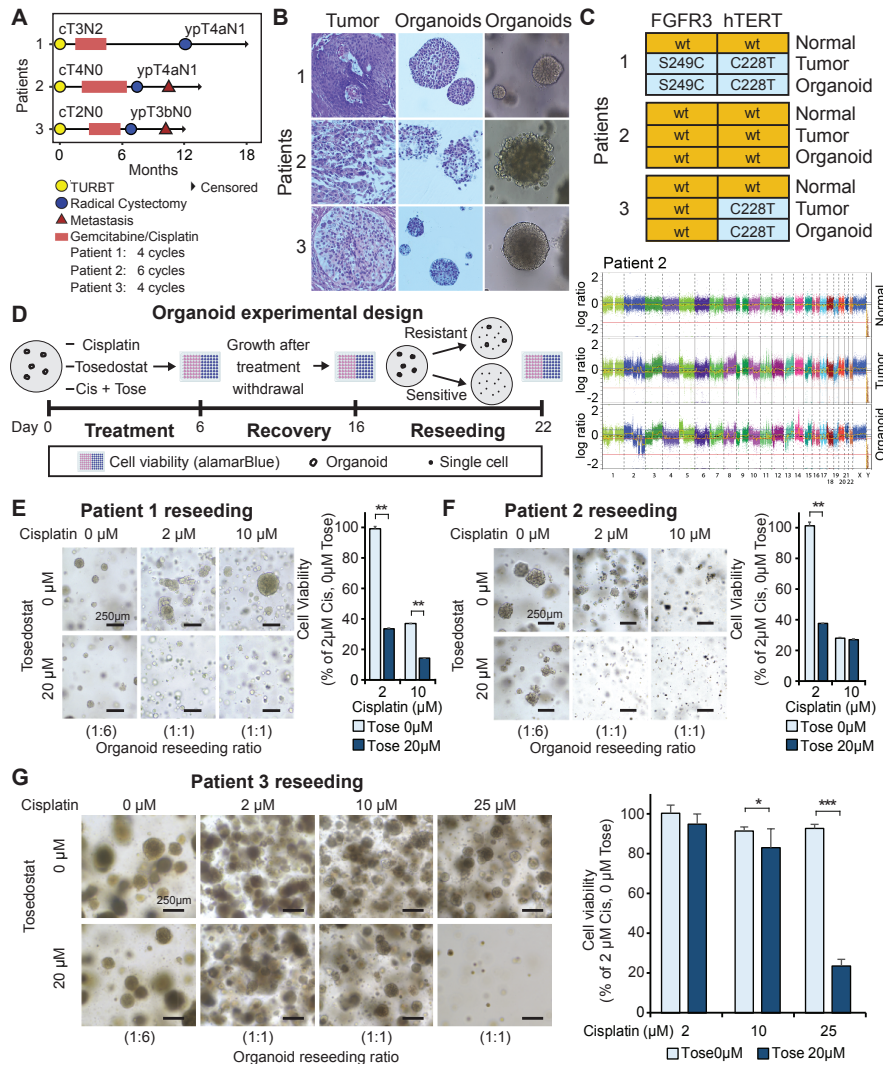
450 Genetic inhibition of NPEPPS enhances chemotherapy sensitivity *in vivo*

451

452 To test if NPEPPS depletion sensitizes tumor cells to gemcitabine plus cisplatin treatment *in*
453 *vivo*, we established subcutaneous xenografts using the KU1919-GemCis cells with either
454 NPEPPS shRNA knockdown or non-targeting shRNA control. When tumors reached roughly
455 200mm³, mice were randomized into four groups: shCtrl1 with PBS (n=11), shCtrl1 with
456 gemcitabine plus cisplatin (n=11), shN39 with PBS (n=11), and shN39 with gemcitabine plus
457 cisplatin (n=12). Treatment was delivered through intraperitoneal injection, with PBS or
458 gemcitabine plus cisplatin administered three times weekly for four weeks. Tumor volumes were
459 monitored until they reached the predetermined endpoint of 2cm³. NPEPPS knockdown alone
460 and gemcitabine plus cisplatin treatment alone had significant impact on tumor growth
461 compared to vehicle-treated, shRNA controls. The combination of NPEPPS knockdown and
462 gemcitabine plus cisplatin treatment led to a stronger and significant impact on tumor growth
463 (**Figure 5H**). We further analyzed tumor growth using linear mixed-effects models aimed at
464 capturing trends in tumor volume change in relation to pre-treatment baseline tumor volume
465 across the four groups (**Figure S10A,B**). According to this model, tumor growth inhibition by
466 NPEPPS knockdown ($p=0.00178$), GemCis treatment ($p=5.49e-7$), or the combination of
467 NPEPPS knockdown and gemcitabine plus cisplatin treatment ($p=1.47e-8$) were all consistent
468 effects over the treatment period (**Figure 5H,I**). We validated NPEPPS knockdown in the pre-
469 xenograft inoculate cells and after tumors were removed from mice upon reaching the 2cm³
470 endpoint (**Figure S10C**). Survival analysis using tumor volume as the endpoint showed that
471 mice treated with gemcitabine plus cisplatin had a 14-day survival advantage. Similarly,
472 knockdown of NPEPPS resulted in a 14-day survival advantage. Mice treated with gemcitabine
473 plus cisplatin and with NPEPPS knockdown tumors had a 25-day survival advantage, a
474 statistically significant improvement (Logrank test, $p<0.0001$) (**Figure 5I**).

475

476 The increase in NPEPPS mRNA that has been observed in response to chronic (**Figure 2B,C**)
477 and acute cisplatin treatment *in vitro* (**Figure 3E**) suggests that high levels of NPEPPS
478 expression are part of an acquired or adaptive rather than intrinsic mechanism of drug
479 resistance in tumors that have been exposed to cisplatin. Hence, pre-treatment tumor NPEPPS
480 levels may not necessarily be a biomarker of chemotherapy response in bladder cancer.
481 However, given the relationship of NPEPPS to VRACs that we describe here and findings that
482 levels of LRRC8A and LRRC8D are predictive of cisplatin response in ovarian cancer (Planells-
483 Cases et al., 2015), we reasoned that such relationships would also be true in BCa. Using
484 TCGA data from muscle-invasive bladder cancer (Robertson et al., 2017), we compared
485 patients with and without a record of platinum-based treatment (Goodspeed et al., 2019) with
486 respect to amplification, copy number, and expression of LRRC8A or LRRC8D. Notably,
487 patients with LRRC8A or LRRC8D copy number gain or overexpression that received cisplatin-
488 based treatment showed significantly improved overall survival in contrast to those with no
489 record of this treatment modality (**Figure 5J,K**). Together, these findings support VRAC
490 subunits LRRC8A and LRRC8D as pre-treatment biomarkers of response to cisplatin-based
491 chemotherapy (Rottenberg et al., 2021).



492
493
494
495
496
497
498
499
500
501
502
503
504
505
506
507
508
509

Figure 6. Pharmacological inhibition of NPEPPS sensitizes ex vivo models of bladder cancer to cisplatin-based chemotherapy. (A) Clinical time course of muscle-invasive bladder cancer patients from whom patient tumor-derived organoid lines were initiated after radical cystectomy. Patients are not lost to follow-up but censored, at the time of publication. TURBT = transurethral resection of bladder tumor. (B) Bright-field images of organoids together with H&E staining of patient tumors and organoids. (C) SNaPshot mutation analysis of patient tumors and organoids on hotspot mutations in fibroblast growth factor receptor 3 (*FGFR3*) or telomerase reverse transcriptase (*TERT*). Copy number plot of the entire genome for the primary tumor and organoids from patient 65 demonstrate the genomic similarity of the tumor-derived organoids. Intensity values of each bin are plotted as colored dots, with each chromosome represented by a different color. (D) Overall experimental design for treating the organoids with cisplatin, tosedostat, or the combination cisplatin plus tosedostat. Organoids were withdrawn from treatment after 6 days of treatment and reseeded after 16 days of treatment. Cell viability was measured using alamarBlue. (E, F, G) Organoids derived from bladder cancer patient tumors that did not respond to gemcitabine plus cisplatin chemotherapy were treated for 6 days with increasing concentrations of cisplatin with or without tosedostat as indicated. Organoids were allowed to recover for 10 days before reseeded of wells to allow for growth of any remaining live cells for an additional 6 days. Cell viability was quantified in triplicate after reseeded (t-test; * $p < 0.05$, ** $p < e^{-3}$, *** $p < e^{-5}$).

510 **Pharmacologic inhibition of NPEPPS enhances chemotherapy sensitivity in** 511 **patient tumor-derived organoids**

512
513 To evaluate our findings in a clinically relevant human model, we extended our work to evaluate
514 the impact of combined cisplatin plus tosedostat on organoid models derived from cystectomy
515 samples from bladder cancer patients that did not respond to gemcitabine plus cisplatin NAC
516 (**Figure 6A**). Based on bladder cancer-specific targeted mutations or global copy number
517 alterations, the organoids had similar characteristics compared to the tumor tissues from which
518 they were derived (**Figure 6B, C**). We treated the organoids with cisplatin plus tosedostat for six
519 days and then removed the drugs to allow recovery for 10 days (**Figure 6D**). Results across
520 increasing doses of cisplatin are reported for all organoids in **Figures S11-S13**. We tested 5 μ M
521 and 20 μ M tosedostat alone and found an initial decrease of roughly 20% due to tosedostat, but
522 over time these cells recovered to equal the vehicle control. With no difference between the two
523 doses, we selected 20 μ M tosedostat for the experiments (**Figure S11D**). After 10 days of
524 recovery from treatment, the drug-treated organoid wells were reseeded as indicated and
525 allowed to grow for an additional 6 days to enable any remaining live treatment resistant cells to
526 grow, then cell viability was assessed (**Figures 6E-G** and **S11-13**). Analogous to a clonogenic
527 assay, organoid reseeded aims to assess the ability of the drug-treated, patient-derived
528 organoids to establish and be a surrogate marker for chemoresistance, outgrowth at secondary
529 sites, and recurrence in patients. Organoids originally treated with increasing concentrations of
530 cisplatin alone resulted in an associated decrease in viability. Those originally treated with
531 cisplatin plus tosedostat resulted in highly significant reductions in viability at 2 μ M in patients 1
532 and 2, and at 25 μ M in the more treatment resistant organoids from patient 3 after reseeded
533 (**Figure 6E-G**). These findings provide validation that tosedostat enhances cisplatin activity in
534 the closest experimental system available short of a human clinical trial.

535 536 **DISCUSSION**

537
538 NPEPPS has been suggested to play a role in a range of cellular processes including promoting
539 autophagy, regulating cell cycle progression, and antigen processing (Constam et al., 1995;
540 Menzies et al., 2010; Saric et al., 2004; Towne et al., 2008). The majority of what is known
541 about NPEPPS has been from studies in the brain, where it targets the degradation of
542 polyglutamine sequences and misfolded protein aggregates associated with a number of
543 neurodegenerative diseases, including Alzheimer's disease, Huntington's disease, and
544 Parkinson's disease (Karsten et al., 2006; Kudo et al., 2011; Menzies et al., 2010; Schönlein et
545 al., 1994; Yanagi et al., 2009). As reported in gnomAD, NPEPPS is a highly conserved gene
546 and constrained based on several metrics of intolerance to genetic variation in the population
547 (Karczewski et al., 2020). NPEPPS is also ubiquitously expressed across human tissues (Uhlen
548 et al., 2017). However, despite these features, genetic modification in mice is tolerable (Osada
549 et al., 1999; Towne et al., 2008) and as we have shown from our CRISPR screen results,
550 knockout is not essential (**Figure 2D**). Overall, NPEPPS presents a viable therapeutic target
551 and we have shown that its downregulation genetically or pharmacologically re-sensitizes
552 treatment-resistant cells back to cisplatin. The mechanism by which NPEPPS controls
553 intracellular import is through VRACs. Direct therapeutic targeting of VRACs will result in
554 treatment resistance, thus our findings represent the first example of targeting VRACs by
555 pharmacological inhibition of NPEPPS.

556
557 Broadly, aminopeptidases have been therapeutically targeted as potential cancer treatments
558 (Hitzerd et al., 2014). More specifically, NPEPPS is a zinc containing M1 aminopeptidase.
559 Tosedostat was developed as a target of M1 aminopeptidases and the intracellular metabolized

560 product CHR-79888 is the most potent inhibitor of NPEPPS reported (Krige et al., 2008; Reid et al., 2009). There have been a total of 11 clinical trials with tosedostat as reported in
561 *clinicaltrials.gov* (Cortes et al., 2013; van Herpen et al., 2010; Krige et al., 2008; Löwenberg et
562 al., 2010; Mawad et al., 2016). The focus of its application has been in leukemias and
563 myelomas, with several applications in solid tumors. The few clinical trials completed have
564 reported tosedostat as being well tolerated by patients, but with modest effect as a cancer
565 treatment alone. A few examples of tosedostat in combination with cytarabine, azacitidine,
566 capecitabine or paclitaxel have been tried, but there are no reports of tosedostat being tried in
567 combination with platinum-based chemotherapy, supporting the novel application of cisplatin-
568 based chemotherapy plus tosedostat that we propose in this study.
569

570
571 Another exciting potential application of NPEPPS inhibition is to provide alternative treatment
572 options for BCa patients. Many patients are ineligible for cisplatin-based chemotherapies,
573 leaving them with less effective options, such as carboplatin. VRACs also transport carboplatin
574 at similar amounts as cisplatin (Planells-Cases et al., 2015), thus combining an NPEPPS
575 inhibitor, such as tosedostat, with carboplatin could provide a more effective and less toxic drug
576 combination option for cisplatin ineligible patients. A further area of novel development would be
577 the impact of NPEPPS inhibition on ICT with its known effect on MHC class I antigen
578 presentation on dendritic cells (Towne et al., 2008). ERAP1 and ERAP2, other M1
579 aminopeptidases in the same family as NPEPPS, have been linked to boosting T cell and NK
580 cell mediated immune response in cancer (Compagnone et al., 2019); however the impact of
581 NPEPPS on antigen presentation in tumor cells is yet to be investigated. Interestingly, low
582 ERAP2 was associated with improved response to anti-PD-L1 in luminal bladder cancer (Lim et
583 al., 2018). The impact of NPEPPS inhibition in immunotherapies requires further study.
584

585 Our results support the role of NPEPPS as an interaction partner that controls cisplatin-based
586 response in BCa via VRACs, thus we have scoped our conclusions accordingly. However,
587 results outside of this study suggest a molecular mechanism with broader impact. The evidence
588 that supports the interaction between NPEPPS and VRACs were derived from several different
589 cell types and the evidence that implicates VRACs in platinum-based chemotherapy sensitivity
590 is from ovarian cancer (Planells-Cases et al., 2015; Sørensen et al., 2014, 2016a, 2016b). If the
591 NPEPPS-VRAC mechanism of platinum-based chemotherapy resistance is a general
592 mechanism, then there are clear implications for any cancer type that uses platinum-based
593 treatments. Hence, we can propose a model (**Figure 7**) where a cancer cell imports cisplatin,
594 which in turn causes DNA damage and eventually cell death. An inherent mechanism of
595 resistance can simply be the number of VRACs in a tumor cell, where downregulation of VRAC
596 subunits can lead to treatment resistance, such as was previously found in ovarian cancer, or
597 the opposite effect seen with LRRC8A or LRRC8D upregulation in BCa (**Figure 5J,K**). In our
598 model, NPEPPS interacts with LRRC8A and/or LRRC8D to inhibit channel activity, thus
599 providing resistance to cisplatin and overall chemoresistance. If proven to be true, our insight
600 into this mechanism opens up opportunities for novel therapeutic strategies to reverse or
601 prevent the development of cisplatin resistance, such as the development of agents that block
602 NPEPPS interactions with VRACs.
603

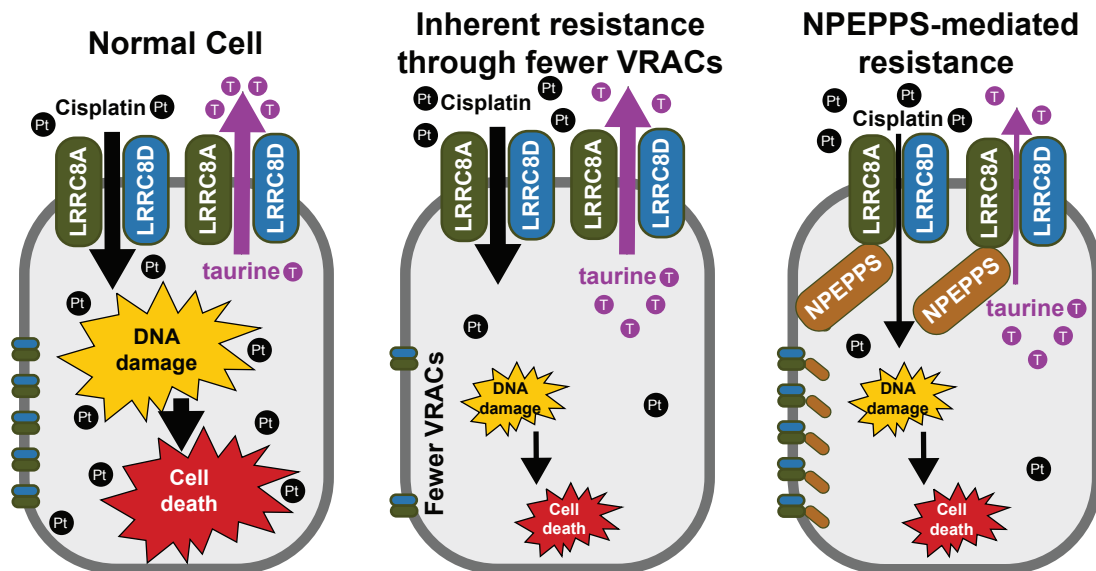
604 This work is not without its limitations. We have shown in multiple settings that inhibiting
605 NPEPPS genetically or pharmacologically results in re-sensitizing resistant BCa cells to
606 cisplatin. However, where and when NPEPPS interacts with VRACs in the cell is yet to be
607 determined. In addition, NPEPPS could have effects on treatment response outside of the
608 VRACs. Our work is also limited by the fact that we have not shown that NPEPPS depletion
609 leads directly to carboplatin sensitization in BCa, but that is likely given the known VRAC
610 relationships (Planells-Cases et al., 2015). Despite these study limitations, the implications of

611 NPEPPS as a therapeutic target for better treatment response has the potential to be translated
612 into novel treatment regimens for improved patient outcomes.

613

614 In conclusion, our finding that NPEPPS mediates cisplatin-based chemoresistance is both novel
615 and actionable. We provided *in vitro*, *in vivo*, and *ex vivo* evidence that this mechanism is robust
616 and therapeutically targetable. Future directions will include determining the detailed
617 mechanism of NPEPPS-mediated treatment response, particularly though the interaction with
618 VRACs, and generating additional preclinical data testing NPEPPS inhibitor efficacy and
619 toxicities. Cisplatin-based chemotherapeutic regimens are mainstays of treatment across many
620 cancer types and these novel findings lay the groundwork for improved treatment of patients
621 harboring these tumors (Rottenberg et al., 2021). Our findings also have implications into other
622 platinum agents, such as carboplatin which would further improve efficacy of this agent in
623 additional cancer types. Finally, for the benefit of the research community, we make the -omic
624 and CRISPR screen data publicly available through an R Shiny app to provide a rich source for
625 novel analysis in the mechanisms of chemotherapy resistance
626 (https://bioinformatics.cuanschutz.edu/BLCA_GC_Omics/).

627



628

629 **Figure 7. Proposed model of NPEPPS-mediated cisplatin resistance.** Normal functioning cells will
630 import cisplatin through the volume regulated anion channels (VRAC), with LRRRC8A and LRRRC8D being
631 the primary subunits. A mechanism of cisplatin resistance is to inherently down-regulate VRACs. We
632 propose that NPEPPS interacts with LRRRC8A or LRRRC8D directly to decrease VRAC activity, which
633 prevents export of taurine and import of cisplatin, hence driving cisplatin resistance.

634 **STAR Methods**

635

636 **Key Resource Table**

REAGENT or RESOURCE	SOURCE	IDENTIFIER
Antibodies		
NPEPPS	Invitrogen	PA5-22383
NPEPPS	Invitrogen	PA5-83788
NPEPPS	Origene	TA308014
GAPDH (D16H11) XP Rabbit mAb	Cell Signaling Technologies	5174S
LRRC8A, Rabbit polyclonal	LSBio	LS-C290818
LRRC8A, Rabbit polyclonal	LSBio	LS-B16989
LRRC8D, Rabbit polyclonal	SinoBiological	104245-T32
Phospho-Histone H2A.X (Ser139) Monoclonal Antibody (3F2)	Invitrogen	MA1-2022
FLAG, monoclonal	Sigma-Aldrich	F1804
Anti-mouse IgG (whole molecule), peroxidase antibody in rabbit	Sigma-Aldrich	A9044
Anti-rabbit IgG (whole molecule), peroxidase-conjugated (HRP)	MP Biomedicals	855689
Bacterial and Virus Strains		
Library Efficiency™ DH5α competent cells	ThermoFisher	18263012
Endura™ ElectroCompetent cells	Lucigen	60242
Chemicals, Peptides, and Recombinant Proteins		
Gemcitabine hydrochloride	Sigma	Y0000675
Gemcitabine hydrochloride (mouse experiment)	BOC Sciences	122111-03-9
Cisplatin	Sigma	PHR-1624
Cisplatin (mouse experiment)	Sigma	11344357
Tosedostat	Sigma	SML2303
Tosedostat (mouse experiment)	BOC Sciences	BCMV18265-2B
Tosedostat (organoids)	Tocris	3595
Puromycin dihydrochloride	Sigma	P9620
Fetal Bovine Serum (FBS)	VWR Seradigm Life Sciences	89510-186
RIPA Lysis and Extraction Buffer	ThermoFisher	89900
T-PER™ Tissue Protein Extraction Reagent	ThermoFisher	PI78510
Halt™ Protease and Phosphatase Inhibitor Cocktail, EDTA-free (100X)	ThermoFisher	PI78443
Polybrene [10mg/mL]	EMD Millipore	TR-1003-G
Lipofectamine 3000 Reagent	ThermoFisher	L3000075
Polyethylenimine, linear (PEI)	Polysciences, Inc.	23966
Lipofectamine® RNAiMAX Reagent	ThermoFisher	13778075
0.5% Trypsin-EDTA (10x)	Gibco	15400-54
DPBS (1x)	Gibco	14190-144
4% formalin	Sigma	HT501128
2.5% Low-Melting Agarose	Sigma	2070
Herculase II Fusion Enzyme	Agilent	600679
DNAseI	Invitrogen	18068015
Deoxynucleotide (dNTP) Solution Mix	New England Biolabs	N0447L

Critical Commercial Assays		
Puregene Cell and tissue Kit	Qiagen	158388
RNase A Solution	Qiagen	158924
SureSelect Human All Exon v6	Agilent	G9611
Amersham ECL Rainbow Marker -Full Range	Sigma	RPN8000E
Precision Plus Protein™ Kaleidoscope™ Prestained Protein Standards	Bio-Rad	1610375
SuperSignal West Pico Plus	ThermoFisher	34580
SuperSignal West Femto	ThermoFisher	34094
4–20% Mini-PROTEAN® TGX™ Precast Protein Gels	Bio-Rad	4561096, 4561094
4X Protein Sample Loading Buffer for Western Blots	LI-COR	928-40004
KAPA library Quant Kit ROX Low	Kapa Biosystems	KK4873
Pierce™ BC Protein Assay Kit	ThermoFisher	23225
Universal Plus mRNA –Seq +UDI kit	Nugen Technologies	9144-96
RNAEasy Plus	Qiagen	74106
QIAmp DNA Mini-Kit	Qiagen	51304
Cell-ID 20-plex Pd Barcoding Kit	Fluidigm	201060
MycoAlert	Lonza	LT07-318
Protein G Sepharose	GE healthcare	GE17-0618-01
Pierce IP lysis bugger	ThermoFisher	87787
SensiFAST Probe No-ROX Mix	Bioline	BIO-86005
SuperScript™ II Reverse Transcriptase	Invitrogen	18064022
NPEPPS TaqMan® Gene Expression Assay	Thermofisher	Hs00196905_m1
HMBS TaqMan® Gene Expression Assay	Thermofisher	Hs00609297_m1
alamarBlue™ Cell Viability Reagent	Invitrogen	DAL 1025
Bio-Rad Protein Assay Dye reagent concentrate	Bio-Rad	5000006
Deposited Data		
Raw RNA sequencing data	This paper	GEO: GSE171537
Raw whole exome sequencing	This paper	SRA: PRJNA714778
Raw CRISPR screen sequencing	This paper	GEO: in progress
Illumina GSA V3 for tumor, adjacent normal, and organoids	This paper	ArrayExpress: E-MTAB-10353
Raw mass spectrometry proteomics	This paper	PRIDE: PXD024742
CRISPR screening results	This paper	Table S13
Bladder tumor proteomics	ProteomeXchange	PXD010260
TCGA bladder cancer patient gene expression	cBioPortal	https://cbioportal-datahub.s3.amazonaws.com/blca_tcga_public_2017.tar.gz
TCGA bladder cancer survival data	(Goodspeed et al., 2019)	Supplementary Table 4
DepMap Common essential and non-essential genes (20Q1)	https://depmap.org/portal/download	common_essentials.csv, nonessentials.csv
Experimental Models: Cell Lines		
T24 parental	Resistant Cancer Cell Line Collection (https://research.kent)	N/A
T24 gemcitabine resistant		N/A
T24 cisplatin resistant		N/A

T24 gemcitabine and cisplatin resistant	ac.uk/industrial-biotechnology-centre/the-resistant-cancer-cell-line-rccl-collection/)	N/A
TCCSUP parental		N/A
TCCSUP gemcitabine resistant		N/A
TCCSUP cisplatin resistant		N/A
TCCSUP gemcitabine and cisplatin resistant		N/A
253J parental		N/A
253J gemcitabine resistant		N/A
253J cisplatin resistant		N/A
253J gemcitabine and cisplatin resistant		N/A
KU1919 parental		N/A
KU1919 gemcitabine resistant		N/A
KU1919 cisplatin resistant		N/A
KU1919 gemcitabine and cisplatin resistant		N/A
5637 parental		N/A
5637 gemcitabine resistant		N/A
5637 cisplatin resistant		N/A
5637 gemcitabine and cisplatin resistant		N/A
293FT	ThermoFisher	R70007
Experimental Models: Organisms/Strains		
Mouse: NU/J	The Jackson Laboratory	002019
Oligonucleotides		
CRISPR screening library primers	This paper	Table S11
Recombinant DNA		
Human CRISPR Knockout Pooled Library (Brunello) - 1 vector system (lentiCRISPRv2)	Addgene	73179
psPAX2	Addgene	12260
pMD2.G	Addgene	12259
shCtrl1	University of Colorado Functional Genomics Facility	SHC002
shCtrl2	University of Colorado Functional Genomics Facility	SHC016
shN38	University of Colorado Functional Genomics Facility	TRCN0000073838
shN39	University of Colorado Functional Genomics Facility	TRCN0000073839
shN40	University of Colorado Functional Genomics Facility	TRCN0000073840
Human NPEPPS siRNA SMARTpool	Horizon Discovery Biosciences Limited	L-005979-00-0020
Human LRRC8A siRNA SMARTpool	Horizon Discovery Biosciences Limited	L-026211-01-0020
Human Non-targeting Pool	Horizon Discovery Biosciences Limited	D-001810-10-20
Software and Algorithms		

BWA-MEM (0.7.17)	(Li, 2013)	http://bio-bwa.sourceforge.net
Samblaster (0.1.24)	(Faust and Hall, 2014)	https://github.com/GregoryFaust/samblaster
Samtools (1.8)/HTSlib (1.9)	(Li et al., 2009)	http://www.htslib.org/
GATK Base Quality Score Recalibration (BQSR)	GATK4 v4.1.8	https://gatk.broadinstitute.org/hc/en-us/articles/360035890531-Base-Quality-Score-Recalibration-BQSR-
Calling Somatic SNVs and Indels with Mutect2	(Benjamin et al., 2019)	https://www.biorxiv.org/content/10.1101/861054v1.full.pdf
Somatic copy number variants	GATK4 v4.1.8	http://genomics.broadinstitute.org/datasheets/PPT_Somatic_CNV_WKST_ASHG_2016.pdf
The Nextflow (20.04.1) pipeline implementing the workflows for this paper	This paper	https://github.com/javidm/layer_lab_vc
SavvyCNV: genome-wide CNV calling from off-target reads v0.10	(Laver et al., 2019)	https://www.biorxiv.org/content/10.1101/617605v1
BBTools	BBMap – Bushnell B. – sourceforge.net/projects/bbmap/	https://jgi.doe.gov/data-and-tools/bbtools/
Image Studio	LiCor	https://www.licor.com/bio/image-studio/
STAR (2.6.0a)	(Dobin et al., 2013)	https://github.com/alexdobin/STAR
FLowJo (10.7.1)	(FlowJo, 2019)	https://www.flowjo.com/
Biodiscovery Nexus CN7.5	N/A	https://www.biodiscovery.com/products/Nexus-Copy-Number
GenomeStudio (1.9.4)	Genotyping Module	https://www.illumina.com/techniques/microarrays/array-data-analysis-experimental-design/genomestudio.html
Limma R package (3.44.3)	(Ritchie et al., 2015)	https://bioconductor.org/packages/release/bioc/html/limma.html
edgeR R package (3.30.3)	(Robinson et al., 2010)	https://bioconductor.org/packages/release/bioc/html/edgeR.html

fgsea R package (1.14.0)	(Sergushichev, 2016)	https://bioconductor.org/packages/release/bioc/html/fgsea.html
ggplot2 R package (3.2.2)	(Wickham, 2009)	https://ggplot2.tidyverse.org/
ggpubr R package (0.4.0)	N/A	https://cran.r-project.org/web/packages/ggpubr/index.html
ClusterProfiler	(Yu et al., 2012)	https://bioconductor.org/packages/release/bioc/html/clusterProfiler.html
caRpoools R package	(Winter et al., 2016)	https://cran.r-project.org/web/packages/caRpoools/index.html
DESeq2 R package	(Love et al., 2014)	https://bioconductor.org/packages/release/bioc/html/DESeq2.html
Maven	(Clasquin et al., 2012)	http://genomics-pubs.princeton.edu/mzroll/index.php
openSWATH	(Röst et al., 2014)	http://openswath.org/en/latest/
vsn (3.12)	(Huber et al., 2002)	https://bioconductor.org/packages/release/bioc/html/vsn.html
lme4 (1.1-26)	(Bates et al., 2015)	https://cran.r-project.org/web/packages/lme4/index.html
lmerTest (3.1-3)	(Kuznetsova et al., 2017)	https://cran.r-project.org/web/packages/lmerTest/index.html
PyProphet	(Teleman et al., 2015)	http://openswath.org/en/latest/docs/pyprophet.html
MSstats R package	(Choi et al., 2014)	https://www.bioconductor.org/packages/release/bioc/html/MSstats.html
TRIC	(Röst et al., 2016)	https://github.com/msproteomicstools/msproteomicstools

637

638 **Cell Culture**

639 All human BCa cell lines as reported in the Key Resource Table were obtained from the
 640 Resistant Cancer Cell Line (RCCL) Collection and were grown in Iscove's Modified Dulbecco's
 641 Medium (IMDM) with 10% Fetal Bovine Serum (FBS). Cells were passaged every two to three

642 days. Resistance to gemcitabine and cisplatin were confirmed at the reported resistance doses
643 from the RCCL (**Table S1** and **Figure S1**). Lentivirus production utilized 293FT cells
644 (ThermoFisher), which were maintained in DMEM (high glucose) supplemented with 0.1mM
645 non-essential amino acids (NEAA), 6mM L-glutamine, 1mM sodium pyruvate, and 500µg/mL
646 geneticin (G418) with 10% FBS added. Cells were routinely monitored for mycoplasma and
647 confirmed negative at multiple times during this study using MycoAlert (Lonza). All cells were
648 grown at 37°C with 5% CO₂ in a humidified incubator.

649 All molecular characterization efforts (RNA sequencing, whole exome sequencing, and mass
650 spectrometric proteomics) were performed on cells from independent passages and in drug-
651 free, complete media to identify stable molecular changes rather than treatment induced
652 transient response. Cells were routinely passaged through drug-containing media at the
653 resistant doses (**Table S1**) to confirm resistance was maintained and early passage cells were
654 utilized whenever possible.

655

656 **RNA sequencing**

657 **Sample preparation**

658 All cell lines were grown for several passages in the absence of antibiotics, gemcitabine or
659 cisplatin. Cell pellets were snap frozen from sub-confluent dishes from 3 separate passages
660 (replicates) for each of the 20 cell lines sequenced (5 cell lines, each with 4 derivatives:
661 parental, G-resistant, C-resistant, GC-resistant). RNA was extracted using the RNAeasy Plus
662 Kit (Qiagen). Cells were lysed and passed through QIAShredder column (Qiagen) according to
663 the manufacturer's protocol. gDNA elimination columns (Qiagen) were used to remove any
664 residual gDNA from the purified RNA. RNA integrity was assessed on the High Sensitivity
665 ScreenTape Assay on the Tape Station2200 (Agilent) and only samples with an RIN score of 8
666 or higher were used for sequencing. RNA library preparation was performed using the Universal
667 Plus mRNA –Seq +UDI kit (Nugen) according to the manufacturer's specification. Each library
668 was sequenced to a minimum of 40 million clusters or 80 million 150bp paired-end reads on a
669 NovaSeq 6000 instrument (Illumina) at the University of Colorado Cancer Center Genomics
670 Shared Resource.

671 **Data processing**

672 Illumina adapters and the first 12 base pairs of each read were trimmed using BBDuk and reads
673 <50bp post trimming were discarded. Reads were aligned and quantified using STAR (Dobin et
674 al., 2013) against the Ensembl human transcriptome (GRCh38.p12 genome (release 96)).
675 Ensembl genes were mapped to HGNC gene symbols using HGNC and Ensembl BioMart.
676 Gene counts were generated using the sum of counts for transcripts of the same gene. Lowly
677 expressed genes were removed if mean raw count <1 or mean CPM (counts per million) <1 for
678 the entire dataset. Reads were normalized to CPM using the edgeR R package (Robinson et
679 al., 2010). Differential expression was calculated using the voom function in the limma R
680 package (Ritchie et al., 2015). In addition to two-group comparisons, single drug comparisons
681 for all cell lines were generated with cell line as a covariate (**Table S7**).

682 **Alignment and transcript quantification**

```
683 STAR --runThreadN 12 --runMode genomeGenerate --sjdbGTFfile  
684 Homo_sapiens.GRCh38.96.gtf --genomeFastaFiles  
685 Homo_sapiens.GRCh38.dna_sm.primary_assembly.fa  
686
```

687 STAR --readFilesIn Read1.fastq.gz Read2.fastq.gz --readFilesCommand zcat --runThreadN 6 --
688 alignEndsProtrude 13 ConcordantPair --outFilterScoreMinOverLread 0.66 --
689 outFilterMatchNminOverLread 0.66 --outSAMtype BAM SortedByCoordinate --quantMode
690 GeneCounts
691

692 **Pathway analysis**

693 Gene set enrichment analysis was performed using the full list of genes ranked by fold change
694 for the indicated comparison and the fgsea R package (Sergushichev, 2016) using gene sets
695 from the Molecular Signatures Database (v7.0) (Liberzon et al., 2011). General plots were
696 generated with the ggplot2 and ggpubr R packages (Wickham, 2009). Heatmaps were
697 generated with the ComplexHeatmap R package following z-score transformation (Gu et al.,
698 2016).

699

700 **Proteomics**

701 ***Sample preparation***

702 All cell lines were grown for several passages in the absence of antibiotics, gemcitabine or
703 cisplatin, then seeded at 100,000 – 200,000 cells per well and grown for 48 hours in IMDM +
704 10% FBS. Approximately 48 hours after seeding cells the supernatant was aspirated and cells
705 were washed 3 times with cold phosphate buffered saline (PBS). Cells were lysed in 100 μ l of
706 8M Urea, 50mM Tris-HCl, pH 8.0. Lysates were transferred to pre-chilled 1.5mL microcentrifuge
707 tubes and centrifuged at 15000 RCF for 10 minutes to pellet. The supernatant was then
708 transferred to a clean, pre-chilled tube and frozen. Lysate replicates were collected in triplicate
709 from different passages. Cell pellets were lysed in 8M Urea supplemented with 0.1% Rapigest
710 MS compatible detergent. DNA was sheared using probe sonication, and protein concentration
711 was estimated by BCA (Pierce, Thermo Scientific). A total of 30 μ g protein per sample was
712 aliquoted, and samples were diluted to <2M Urea concentration using 200mM ammonium
713 bicarbonate while also undergoing reduction with DTT (10mM) and then alkylation with IAA
714 (100mM). The pH of diluted protein lysates was verified as between 7-8, and samples were
715 digested with sequencing grade Trypsin/Lys-C enzyme (Promega) in the presence of 10%
716 Acetonitrile for 16 hours at 37°C. Samples were acidified adding formic acid to 1%, and speed
717 vac dehydration was used to evaporate acetonitrile. Peptides were desalted on C18 tips (Nest
718 group) and dried to completion. Prior to MS, peptides were resuspended in 0.1% Formic Acid
719 solution at 0.5 μ g/ μ L concentration with 1:40 synthetic iRT reference peptides (Biognosys).

720 ***Data acquisition***

721 Peptides were analyzed by liquid chromatography coupled with mass spectrometry in data
722 independent acquisition (DIA) mode essentially as described previously (Robinson et al., 2020).
723 Briefly, 4 μ L of digested sample were injected directly unto a 200 cm micro pillar array column
724 (uPAC, Pharmafluidics) and separated over 120 minutes reversed phase gradient at 1200
725 nL/min and 60°C. The gradient of aqueous 0.1% formic acid (A) and 0.1% formic acid in
726 acetonitrile (B) was implemented as follows: 2% B from 0 to 5 min, ramp to 4% B at 5.2 minutes,
727 linear ramp to 28% B at 95 minutes, and ramp to 46% B at 120 minutes. After each analytical
728 run, the column was flushed at 1200 nL/min and 60°C by injection of 50% Methanol at 95% B
729 for 25 minutes followed by a 10 minutes ramp down to 2% B and a 5 minute equilibration to 2%
730 B. The eluting peptides were electro sprayed through a 30 μ m bore stainless steel emitter
731 (EvoSep) and analyzed on an Orbitrap Lumos using data independent acquisition (DIA)
732 spanning the 400-1000 m/z range. Each DIA scan isolated a 4 m/z window with no overlap

733 between windows, accumulated the ion current for a maximum of 54 seconds to a maximum
734 AGC of 5E5, activated the selected ions by HCD set at 30% normalized collision energy, and
735 analyzed the fragments in the 200-2000m/z range using 30,000 resolution (m/z = 200). After
736 analysis of the full m/z range (150 DIA scans) a precursor scan was acquired over the 400-1000
737 m/z range at 60,000 resolution.

738 ***Peptide library generation***

739 To construct a comprehensive peptide ion library for the analysis of human BCa we combined
740 several datasets, both internally generated and external publicly available data resources were
741 utilized. First, we utilized a previously published (Berle et al., 2018) human bladder tumor
742 proteomics experiment by downloading raw files from the online data repository
743 (ProteomeXchange, PXD010260) and searching them through our internal pipeline for data
744 dependent acquisition MS analysis (Parker et al., 2016) against the UniProt human reviewed
745 canonical sequence database, downloaded July 2019, using internal peptides to perform
746 retention time alignment (Parker et al., 2015). To this library, we appended a sample specific
747 library generated from DIA-Umpire extraction of pseudo-spectra from one full set of replicates
748 from the experimental bladder tumor cell lines. A final, combined consensus spectrast library
749 containing all peptide identifications made between the internal and external dataset was
750 compiled and decoy sequences were appended.

751 ***Data analysis***

752 Peptide identification was performed as previously described in (Parker et al., 2015, 2016).
753 Briefly, we extracted chromatograms and assigned peak groups using openSWATH (Röst et al.,
754 2014) against the custom BCa peptide assay library described above. False discovery rate for
755 peptide identification was assigned using PyProphet (Teleman et al., 2015) and the TRIC (Röst
756 et al., 2016) algorithm was used to perform feature-alignment across multiple runs of different
757 samples to maximize data completeness and reduce peak identification errors. Target peptides
758 with a false discovery rate (FDR) of identification <1% in at least one dataset file, and up to 5%
759 across all dataset files were included in the final results. We used SWATH2stats to convert our
760 data into the correct format for use with downstream software MSstats (Choi et al., 2014). Each
761 individual data file was intensity normalized by dividing the raw fragment intensities to that files
762 total MS2 signal. MSstats (Choi et al., 2014) was used to convert fragment-level data into
763 protein-level intensity estimates via the 'quantData' function, utilizing default parameters with the
764 exception of data normalization, which was set to 'FALSE'. For plotting purposes, protein
765 intensities were VSN normalized, log-transformed, and replicate batch effects were removed
766 using the removeBatchEffect function in the limma R package. The limma package was also
767 used to calculate differential protein expression (Ritchie et al., 2015). Multiple hypothesis
768 correction was performed using the Benjamin Hochberg method.

769

770 ***Whole exome sequencing***

771 ***Sample preparation***

772 All cell lines were grown for several passages in the absence of antibiotics, gemcitabine or
773 cisplatin. Cell pellets were snap frozen from sub-confluent dishes for each of the 20 cell lines
774 sequenced (5 cell lines, each with 4 derivatives: parental, Gem-resistant, Cis-resistant, GemCis-
775 resistant). gDNA isolation was performed using the Puregene cell and tissue kit (Qiagen) with
776 the addition of RNase A Solution (Qiagen) according to manufacturer's instructions. gDNA was
777 quantified using a Qubit 4.0, then sheared using a Covaris S220 Sonicator to 200bp. Libraries
778 were constructed using the Sure Select All Exon v6 library kit (Agilent) following the XT library
779 preparation workflow. Completed libraries were run on the 4200 Tape Station (Agilent) using

780 D1000 screen tape. Libraries were quantitated using the Qubit, diluted to 4nM prior to
781 verification of cluster efficiency using qPCR, then sequenced on the NovaSeq 6000 instrument
782 (Illumina) (150bp, paired-end) at the University of Colorado Cancer Center Genomics Shared
783 Resource. Mean insert size across all cell lines was 177.8 bp and mean coverage was 193.7X
784 with > 96.8% at >30X. Individual call line quality control metrics are reported in **Table S12**.

785 **Data processing**

786 The analysis pipeline was developed using Nextflow. For the raw fastq files, Fastqc was used to
787 assess overall quality. For computational efficiency, raw sequence reads were partitioned using
788 BMap (partition.sh) into 40 partitions. They then were aligned to the GRCh38 reference
789 genome (including decoy sequences from the GATK resource bundle) using the BWA-MEM
790 short read aligner (Li, 2013), and merged back into single BAM files using Samtools. The
791 resulting BAM files were de-duplicated using Samblaster (Faust and Hall, 2014), and sorted
792 using Samtools. These duplicate-marked bams were further passed through the GATK Base
793 Quality Score Recalibration in order to detect systematic errors made by the sequencing
794 machine when it estimates the accuracy of base calls. The dbSNP (version 146) (Sherry et al.,
795 2001), the 1000 Genome Project Phase 1 (1000 Genomes Project Consortium et al., 2015), and
796 the Mills and 1000G gold standard sets (Mills et al., 2011) were used as databases of known
797 polymorphic sites to exclude regions around known polymorphisms from analysis. After
798 alignment, Samtools (Li et al., 2009), Qualimap (Okonechnikov et al., 2016), and Picard tools
799 (2018) were run to acquire various metrics to ensure there were no major anomalies in the
800 aligned data.

801 **Alignment**

802 `bwa mem -K 100000000 -R "read_group" -t 64 -M ref_fasta read_1 read_2`

803 **Marking duplicates**

804 `samtools sort -n -O SAM sample_bam | samblaster -M --ignoreUnmated`

805 **Base Quality Score Recalibration**

806 `gatk BaseRecalibrator -I sample_bam -O sample.recal.table -R ref_fasta --known-sites`
807 `known_sites`

808 **Whole exome sequencing variant calling**

809 We used Mutect2 from the GATK toolkit for SNVs and short indels (Benjamin et al., 2019).
810 Mutect2 is designed to call somatic variants and makes no assumptions about the ploidy of
811 samples. It was run in *tumor-only* mode to maximize the sensitivity albeit at the risk of high false
812 positives. We used tumor-only mode to call variants for each cell line separately. Mutect2
813 workflow is a two steps process. In the first step, it operates in high sensitivity mode to generate
814 intermediate callsets that are further subjected to filtering to generate the final variant calls.
815 Annotation of variants was performed using Annovar (Wang et al., 2010) with the following
816 databases: refGene, cytoBand, exac03, avsnp150, clinvar_20190305, gnomad211_exome,
817 dbnsfp35c, cosmic90. Intergenic variants were removed along with variants that were identified
818 at greater than 0.001% of the population according to ExAC or gnomAD, or had a depth < 20.

819 **Mutect2 raw callset:**

820 `gatk Mutect2 -R ref_fasta -I bam_tumor -tumor Id_tumor --germline-resource germline_resource`
821 `-O raw_vcf`

822 **Mutect2 filtering:**

823 `gatk FilterMutectCalls -V raw_vcf --stats raw_vcf_stats -R ref_fasta -O filtered_mutect2_vcf`

824 **Copy number calling using GATK**

825 Base quality score recalibrated bam files were used as the input. The covered regions for the
826 exome kit were converted into bins (defining the resolution of the analysis) for coverage
827 collection. Read-counts, that form the basis of copy number variant detection, were collected for
828 each bin. The read-counts then go through denoising, modelling segments, and calling the final
829 copy ratios.

830 **Preprocess intervals**

```
831 gatk PreprocessIntervals --intervals intervals_bed_file --padding 0 --bin-length 0 -R ref_fasta --  
832 interval-merging-rule OVERLAPPING_ONLY -O preprocessed_intervals_list
```

833 **Collect read counts**

```
834 gatk CollectReadCounts -I sample_bam -L preprocessed_intervals} --interval-merging-rule  
835 OVERLAPPING_ONLY -O sample.counts.hdf5
```

836 **Denoise read counts**

```
837 gatk DenoiseReadCounts -I sample.counts.hdf5 --standardized-copy-ratios  
838 sample_std_copy_ratio --denoised-copy-ratios sample_denoised_copy_ratio
```

839 **Model Segments**

```
840 gatk ModelSegments --denoised-copy-ratios denoised_copy_ratio --output-prefix id_sample -O  
841 output_dir
```

842 **Call copy ratio segments**

```
843 gatk CallCopyRatioSegments -I sample.modelled_segments -O sampled.called.segments
```

844 **Cell line authentication**

845 Variant calls from the Mutect2 pipeline were filtered for each cell line to identify high confidence
846 variants according to the filtering criteria above. These high confidence variants were then
847 compared to the variants reported for all cell lines in the DepMap (<https://depmap.org/portal/>) for
848 the Cancer Cell Line Encyclopedia (CCLE_mutations_hg38.csv, sample_info.csv) and COSMIC
849 (CosmicCLP_MutantExport.tsv) as measured by the jaccard distance, the intersection of
850 variants divided by the union of variants. Cells listed in CCLE or COSMIC were the rank ordered
851 for each BCa cell line in this study according to the jaccard distance. Results are reported in
852 **Table S13**.

853

854 **Metabolomics**

855 **Sample preparation**

856 Cell lines were cultured for several passages in IMDM + 10% FBS (IMDM10). Prior to
857 experiment, cells were cultured in IMDM10 to ~80% confluence and then dissociated. For
858 dissociation, cells were washed once with room temperature PBS and then incubated with PBS
859 + 0.05% Trypsin-EDTA for 10-15 minutes. Cells were neutralized with IMDM10 and then fully
860 dissociated by gentle pipetting. After dissociation, cells were counted by Trypan blue staining
861 and then replated at 1e6 cells. 24 hours after plating, cells were treated with either IMDM10 or
862 IMDM10 + 10 μ M cisplatin. Day 0 cell cultures were immediately processed for metabolomics
863 analysis. To prepare cell pellets for metabolomics analysis, day 0 cells were dissociated and
864 then centrifuged at 300RCF for 10 minutes at 4°C. Cells were suspended in PBS, centrifuged a
865 second time, and then resuspended in PBS and counted. Day 0 cells were centrifuged a third
866 time, the supernatants were aspirated, and the dry cell pellets were snap frozen in liquid

867 nitrogen and stored at -80°C until metabolite extraction. 72 hours after plating, cells were
868 processed for metabolomics analysis as described for the day 0 cell cultures.

869 **Data generation and analysis**

870 Metabolites from frozen cell pellets were extracted at 2e6 cells/mL in ice cold 5:3:2
871 MeOH:acetonitrile:water. Extractions were carried out using vigorous vortexing for 30 min at
872 4°C. Supernatants were clarified by centrifugation (10 min, 18,000 g, 4°C) and 10 µL analyzed
873 using a Thermo Vanquish UHPLC coupled to a Thermo Q Exactive mass spectrometer. Global
874 metabolomics analyses were performed using a 5 min C18 gradient in positive and negative ion
875 modes (separate runs) with electrospray ionization as described in (Gehrke et al., 2019;
876 Nemkov et al., 2019). For all analyses, the MS scanned in MS¹ mode across the m/z range of
877 65 to 950. Peaks were annotated in conjunction with the KEGG database, integrated, and
878 quality control performed using Maven as described in (Nemkov et al., 2015). Data was
879 variance stabilization normalized (Huber et al., 2002), log₂-transformed, and differential
880 abundance calculations were done using limma (Ritchie et al., 2015) with time and/or treatment
881 as covariates in the linear model.

882

883 **Cell Line Drug Treatments**

884 Gemcitabine (Sigma) and cisplatin (Sigma) stocks were resuspended in 0.9% saline solution
885 and tosedostat (Sigma and BOC Sciences) was resuspended in DMSO. All stocks solutions
886 were stored protected from light and kept frozen until use. For cell culture dose response, cells
887 were seeded in 96-well tissue culture plates with 500-2000 cells per well depending on growth
888 rate and duration of experiment. Cells were seeded and allowed to attach overnight followed by
889 replacing the media with fresh, pre-warmed media just prior to treatment. Drug dilutions were
890 performed serially and using complete media (IMDM + 10% FBS) and the associated drug
891 treatments. Growth inhibition was measured using confluence estimates over time on the
892 IncuCyte ZOOM (Essen Bioscience) over varying amounts of time depending on each
893 experiment. Details for timing and replicates for each experiment are included in their respective
894 figure legends.

895

896 **Antibodies and Western Blotting**

897 Whole cell lysates were prepared from cultured cells using RIPA lysis and extraction buffer
898 (ThermoScientific). Lysates from xenograft tissues were prepared using tissue protein extraction
899 reagent (T-PER) and glass tissue homogenizer. All lysates were prepared on ice and with the
900 addition of Halt protease and phosphatase inhibitor cocktail and EDTA (ThermoFisher). Protein
901 concentration of lysates were quantified with BCA protein assay (Pierce™, ThermoFisher). All
902 lysates were prepared with 4X Licor Loading buffer with DTT added boiled for 10 minutes prior
903 to gel loading. All western blots were run using PROTEAN TGX precast 4-15% or 4-20%
904 gradient gels (Bio-Rad) and transferred to either 0.2µm or 0.44µm nitrocellulose membranes.
905 Transfer was done for 1.5-2hrs in cold TrisGlycine buffer (Bio-Rad) with 20% methanol prior
906 blocking for 1hr at room temperature in 5% BSA in TBS-T. Primary antibodies were diluted and
907 incubated overnight at 4°C on a rocker. Membranes were washed 3 or 4 times in fresh TBS-T
908 prior a 1 hour room temperature incubation in an appropriate secondary antibody. Membranes
909 were washed 3-4 times in TBS-T, developed with enhanced SuperSignal West Pico Plus or
910 SuperSignal West Femto (ThermoFisher) and imaged using Li-Cor Odyssey® Fc instrument.
911 Densitometry was performed using LiCor Image Studio™ software. Statistical comparisons
912 using densitometry measurements were done using a one-way ANOVA with Tukey post hoc to
913 control for the experiment-wise error rate.

914

915 **Immunoprecipitation**

916 Immunoprecipitation of human bladder cancer cell lines was carried out using Protein G
917 Sepharose beads following manufacturer protocol (GE healthcare). Cells were lysed using Pierce
918 IP lysis buffer containing 25 mM Tris HCL pH 7.4, 150mM NaCl, 1% NP-40, 1 mM EDTA, 5%
919 glycerol added with phosphatase and protease inhibitor mixture (Roche Applied Sciences).
920 Sepharose beads slurry has been washed three times with the lysis buffer by centrifuging at 3,000
921 x g for 2 min at 4°C. Then conjugated anti-FLAG antibody was carried out by overnight incubation
922 of the suspended Protein G Sepharose and anti-Flag monoclonal antibody (Sigma F1804) at 4°C
923 with continuous mixing. After three-time washing with lysis buffer, the mixture was incubated with
924 the lysates at 4°C overnight with gentle mixing on a suitable shaker. Next, the precipitated protein
925 with the bead was washed three times and analyzed using the immunoblotting technique as
926 described (Agarwal et al., 2016). Whole-cell lysate has been used for input or positive control.
927 Anti-FLAP pull down was performed for FLAG non-expressing bladder cancer cell line for negative
928 control. NPEPPS and LRRC8A has been probed using Rabbit polyclonal NPEPPS antibody
929 (1:1000; Origene), Rabbit IgG polyclonal LRRC8A antibody (1:1000, LSBio) and Rabbit IgG
930 polyclonal LRRC8D antibody (1:1000, SinoBiological).
931

932 **Cisplatin induced NPEPPS mRNA expression**

933 Total RNA was isolated from cells using Trizol (ThermoFisher) and standard phenol-chloroform
934 based extraction methods. Residual DNA was digested with DNase I (Life technologies). cDNA
935 synthesis was performed using Superscript II Reverse Transcriptase kit (Life technologies)
936 using random primers. RT-qPCR reactions were performed on a CFX Connect Real-Time PCR
937 Detection System thermocycler (Bio-Rad) using TaqMan™ gene expression assays for
938 NPEPPS and HMBS as a housekeeping gene (ThermoFisher) in combination with
939 SensiFAST™ Probe No-ROX Kit (Bioline, Toronto, Canada). Expression data was calculated
940 using $2^{-\Delta\Delta Ct}$. All cell line experiments were performed in triplicate from independently grown
941 cells. Comparisons at the indicated dose of cisplatin were made to the control treatment (0μM
942 cisplatin) using a t-test.

943

944 **siRNA-mediated knockdown experiments**

945 NPEPPS and non-targeting siRNA SMARTpools were purchased from Horizon Discovery and
946 resuspended in Dharmacon 5X siRNA Buffer. Transfections were performed using
947 Lipofectamine RNAiMax (ThermoFisher) transfection reagent according to the manufacturer's
948 specifications. Briefly, cells were grown to ~60% confluence in 6-well plates prior to being
949 transfected and allowed to incubate overnight. The following day cells were trypsinized and
950 replated into 96-well plates at 1000-2000 cells per well and allowed to attach overnight. Cells
951 from the initial transfection were also replated into 6-well plates to collect protein and RNA to
952 confirm knockdown. The following day, cells were treated using their previously established
953 resistance doses of gemcitabine, cisplatin, or gemcitabine plus cisplatin (**Table S1**), and their
954 relative growth rates were measured on the IncuCyte ZOOM (Essen Bioscience) over time. For
955 the CyTOF experiments, cells were grown in siRNA SMARTpools for 72 hours before beginning
956 cisplatin treatment.

957

958 **shRNA-mediated knockdown experiments**

959 Lentiviral production and transduction were carried out by the University of Colorado Cancer
960 Center Functional Genomics Shared Resources. Plasmids from The RNAi Consortium (TRC)
961 collection (TRC construct numbers TRCN0000073838, TRCN0000073839 and
962 TRCN0000073840) were used for targeting NPEPPS were selected based on predicted
963 knockdown efficiency; non-targeting controls used were SHC002 and SHC016. 2 μ g of target
964 shRNA construct and 2 μ g of 3:1 ratio of psPAX2 (Addgene) and pMD2.G (Addgene) were
965 transfected into HEK293FT cells using 2 μ g of Polyethylenimine (Polysciences). Lentiviral
966 particle containing media was filtered using 0.45 μ m cellulose acetate syringe filter and used for
967 transduction. Puromycin selection was performed at doses used for CRISPR library screening
968 or in some cases, cells were re-selected with higher doses of puromycin (10 μ g/mL), in order to
969 ensure complete elimination of non-transduced cells. Selected cells were frozen at early
970 passage and early passage cells were used for all experiments.

971

972 **Intracellular cisplatin measurements using CyTOF**

973 Cell lines were cultured for several passages in IMDM + 10% FBS. Prior to experiment, cells
974 were cultured in IMDM10 to be 50-80% confluence overnight and then treated the next day with
975 varying concentrations of cisplatin or PBS as indicated and then dissociated after 4 hours of
976 treatment. For dissociation, cells were washed twice with room temperature PBS and then
977 incubated with PBS + 0.05% Trypsin-EDTA for 10-15 minutes. Cells were neutralized with
978 IMDM10 and then fully dissociated into single-cell suspension by gentle pipetting. After
979 dissociation, cells were counted by Trypan blue staining and then placed in separate tubes at 3
980 x 10⁵ cells. Individual samples were then fixed, permeabilized, and labeled using unique
981 barcodes using the Cell-ID 20-plex Pd Barcoding kit (Fluidigm) according to the manufacturer
982 protocol. Barcoded samples were pooled across cell line condition and cisplatin concentration,
983 incubated with Cell-ID Intercalator-Ir, mixed with equilibration beads and acquired on a Helios
984 mass cytometer (Fluidigm). Post-acquisition data were normalized to equilibration beads and
985 debarcoded, using the bead-normalization and single-cell-debarcoder packages from the Nolan
986 Laboratory GitHub page (<https://github.com/nolanlab>). Relative cisplatin intensity (defined by
987 ¹⁹⁵Platinum isotopic mass intensity) was analyzed among nucleated ¹⁹¹Iridium+ ¹⁹³Iridium+
988 events defined by Boolean gating within FlowJo 10.7.1.

989

990 **Whole Genome CRISPR Screening**

991 ***Plasmid library expansion and quality control***

992 Whole genome CRISPR Screening was performed using the Human CRISPR Knockout Pooled
993 Library (Brunello) - 1 vector system (Addgene and a gift from John Doench to the Functional
994 Genomics Facility at the University of Colorado Anschutz Medical Campus) (Doench et al.,
995 2016). Two distinct plasmid expansions were performed. And the library distribution was
996 assessed using next generation sequencing to determine the impact on overall library was
997 modest following re-expansion. Library width was calculated as previously described (Imkeller et
998 al., 2020; Joung et al., 2017) by dividing the 10th percentile of the library distribution by the 90th
999 percentile using the log2 average expression of all sgRNAs in the library and found to be 6.7
1000 and 7.13 for batch 1 and 2 respectively. All quality control metrics for each sample are reported
1001 in **Table S14**. Different screening parameters were used based on the cell line screened these
1002 are summarized in **Table S4**.

1003 **Lentivirus Production and Titration**

1004 For the two plasmid batches, two distinct protocols for lentivirus production were utilized. The
1005 first batch was generated by using Polyethylenimine, linear (PEI; Polysciences) and was used
1006 for the T24-GemCis and TCCSUP-GemCis screens. The second used lipofectamine 3000 and
1007 was applied for the 253J-GemCis, KU1919-GemCis, and 5637-GemCis screens. For the first
1008 batch, 293FT cells were seeded at a density of 36,800 cells/cm² into a 4-layer CELLdisc
1009 (Greiner) using DMEM + 10% FBS along with antibiotic and antimycotic solution. Transfection
1010 mix consisting 47.6µg pMD2G (Addgene), 95.2µg of psPAX2 (Addgene), and 190.5µg of
1011 Brunello Whole genome knockout library (Addgene) was mixed with 448µl PEI (1 mg/mL) and
1012 3mL OptiMEM, vortexed for 30 seconds and allowed to incubate at room temperature for 20
1013 minutes. Fresh media containing transfection mix were added to the CELLdisc using up to
1014 270mL of media. The next day media was changed for 280mL fresh media followed by a 48-
1015 hour incubation. After this 48-hour incubation the viral supernatant was harvested and filtered
1016 through a cellulose acetate filter system (ThermoScientific) and frozen at -80°C.

1017 The first method had low functional virus titer, so we implemented a different virus production
1018 method for subsequent screens. In the second batch of virus production, we utilized
1019 lipofectamine 3000 instead of PEI, eliminated use of multilayer flasks and centrifuged to remove
1020 debris as opposed to filtering. Briefly, 293FT cells were plated in T225 flasks to be 80%
1021 confluent after 24hrs. 2hrs before transfection, media was changed and 40mL of fresh media
1022 was used per T225 flask. The lipofectamine 3000 protocol was followed according to
1023 manufacturer's instructions and scaled based on the volume of virus being prepared. For each
1024 T225 flask 2mLOptiMEM was mixed with 40µg Brunello whole genome library plasmid, 30µg of
1025 psPAX2 and 20µg of pMD2.G and 180µl of P3000. This mix was added to a tube containing
1026 2mL OptiMEM and 128µl Lipofectamine 3000, which was scaled according to the number of
1027 T225 flasks being prepared. Transfection mix was mixed thoroughly by pipetting up and down
1028 slowly, and allowed to incubate at room temperature for 15 minutes. Transfection mix was then
1029 added dropwise to the plates of 293FT cells with gentle swirling and incubated overnight
1030 (~16hr). The following morning, the media was changed and 60mL of fresh media was added to
1031 each T225 flask. This was allowed to incubate overnight and replaced the following morning.
1032 This first lentiviral supernatant was stored at 4°C to be pooled with a subsequent 48 hour
1033 collection. Upon collection, viral supernatants had 1M HEPES added at 1%. Following the
1034 second virus collection, supernatants were pooled and centrifuged at 1250rpm for 5 minutes to
1035 pellet debris. Lentivirus was stored in polypropylene tubes as polystyrene is known to bind
1036 lentivirus, and all tubes were flash frozen in liquid nitrogen and stored at -80°C. Despite the
1037 changes to the lentiviral production protocols, functional lentiviral titers were not improved using
1038 these changes to the methodology, but feel it is worth noting these changes in protocol to
1039 account for any possible variability associated with this change.

1040 Lentivirus was titered functionally based on protocols adapted from the Broad Institute's Genetic
1041 Perturbation Platform's public web portal (<https://portals.broadinstitute.org/gpp/public/>).

1042 **Screening Parameter Optimization**

1043 All screening parameters for each cell lines including cell polybrene and puromycin sensitivity,
1044 screening coverage, technical and biological replicates performed, and gemcitabine and
1045 cisplatin treatment concentrations are reported in **Table S4**.

1046 **DNA Isolation**

1047 Cell pellets of 2e7 were snap frozen in liquid nitrogen in 1.5mL tubes and stored at -80 prior to
1048 extraction. When possible at least 8e7 cell were used for 4 separate genomic DNA isolation
1049 which were pooled to account for any variation with pellet size. DNA isolation was performed

1050 using the Puregene cell and tissue kit (Qiagen) with the addition of RNase A Solution (Qiagen)
1051 according to manufacturer's instructions. DNA concentration was measured in quadruplicate
1052 using either a nanodrop spectrophotometer (Thermo), Qubit® dsDNA assay (Life Technologies)
1053 and the average DNA content per cell was determined.

1054 ***Library preparation***

1055 The minimum number of cell equivalents of gDNA to maintain equal coverage was used for
1056 library preparation. In all screens, the minimum coverage based on cell number was multiplied
1057 by the average gDNA content per cell for each individual cell line to determine the minimum
1058 number for 10µg PCR reactions needed to maintain coverage. A minimum coverage of 500-fold
1059 per sgRNA in the library was targeted for each independent sample or replicate but this was
1060 increased in some cases where screening was carried out with greater depth (see **Table S4** for
1061 coverage and replicate information).

1062 Library preparation was performed using primers sequences designed by the Broad Institute's
1063 Genetic Perturbation Platform (<https://portals.broadinstitute.org/gpp/public/>) and utilized a pool
1064 of eight P5 primers with to introduce a stagger in reads associated with each library and sample
1065 specific P7 primer that contained a unique sample index sequence for each timepoint, replicate,
1066 or treatment condition to be sequenced in the same pool (**Table S11**). All library preparation
1067 primers were resuspended at 100µM.

1068 Each library preparation PCR reaction contained the following components: 1µl Herculase II
1069 Fusion Enzyme (Agilent), 2.5µl Deoxynucleotide (dNTP) Solution Mix (New England Biolabs),
1070 0.5µl P5 primer pool, 0.5µl P7 index primer, 20µl 5X Reaction Buffer (Agilent), 10µg of gDNA
1071 and nuclease-free water to bring the total reaction volume to 100µl. Samples underwent 23
1072 cycles of thermal cycling followed by a quality assessment by electrophoresis on 2% agarose
1073 gel to ensure consistent library amplification across multiple wells and samples for each plate.

1074 Each unique library had 10µl pooled from all PCR reactions performed on that unique sample
1075 and mixed thoroughly. 50-100µl of the pooled library preparation reactions was used to perform
1076 magnetic bead-based purification and elimination of any residual free primer using a 0.8X ratio
1077 SPRIselect beads (Beckman Coulter) according to the manufacturer's instructions. Libraries
1078 were then assessed for appropriate amplicon size and complete elimination of free primer peaks
1079 using the High Sensitivity ScreenTape Assay on the Tape Station2200 (Agilent) and quantified
1080 using the qPCR-based quantification in order to ensure only NGS-compatible amplicon was
1081 quantified using the Library Quant ROX Low Kit (Kapa Biosystems) on a QuantStudio™ 6
1082 Realtime PCR System (ThermoFisher). Following qPCR quantification, all libraries were
1083 normalized to a standard concentration (typically 20-40nM) depending on the lowest
1084 concentration library to be pooled, and then requantified by qPCR to ensure all samples were
1085 within ~10-20% of the pool mean target concentration. After confirming accurate library
1086 quantification and normalization, samples were pooled at an equimolar ratio and submitted for
1087 sequencing. Libraries were sequenced on the NovaSeq 6000 instrument (Illumina) (150bp,
1088 paired-end) at the University of Colorado Cancer Center Genomics Shared Resource.

1089 ***CRISPR screening bioinformatic pipeline and analysis***

1090 sgRNA counts were extracted directly from R1 raw sequence reads using a custom perl script
1091 that uses regular expression string matching to exactly match sgRNA sequence flanked by 10
1092 bases of vector sequence. The vector sequence was allowed to have one error before and after
1093 the sgRNA sequence. sgRNAs were tabulated for each sample based on the sgRNA sequence
1094 (**Table S15**). The sgRNA IDs of the Brunello library were updated to current HGNC gene names
1095 using the Total Approved Symbols download from HGNC, accessed on 9/1/2020
1096 (<https://www.genenames.org/download/statistics-and-files/>). Transcript IDs were matched when

1097 possible and when matches were not found, past symbols and aliases were updated to current
1098 names. Finally, 5 sgRNAs with missing updated gene names were manually curated using
1099 literature searches. Library distribution was calculated using the caRools R package (Winter et
1100 al., 2016) (**Table S11**). The DESeq2 R package (Love et al., 2014) was used to calculate
1101 differential abundance of genes (**Table S5**). Gene counts were generated using the sum of
1102 counts for sgRNAs of the same gene. Synthetic lethality compared GemCis day 19 and GemCis
1103 day 25 vs. PBS day 19 and PBS day 25 with the day as a covariate. In the comparison
1104 integrating all cell lines, cell line was additionally modeled as a covariate. Gene essentiality was
1105 calculated by comparing PBS day 25 to PBS day 0 and in the integrated all cell lines
1106 comparison; cell line was modeled as a covariate. Common synthetic lethal genes were defined
1107 as being statistically significantly differentially lost (FDR < 0.05 and Log2 FC < 0) in each of the
1108 5 cell lines. Gene set enrichment analysis (GSEA) was performed using the fgsea R package
1109 run with 10000 permutations (Sergushichev, 2016) with the KEGG and Reactome gene sets
1110 from MSigDB (Liberzon et al., 2011). Heatmaps were generated with the ComplexHeatmap R
1111 package following z-score transformation (Gu et al., 2016). Other plots were generated using
1112 the ggplot2 R package.

1113 **Xenograft experiments**

1114 Six-week-old, female NU/J mice (Jackson Labs) were allowed to acclimate for at least one week
1115 prior to initiating any experiments. Mice had free access to food and water in pathogen-free
1116 housing and cared for in accordance NIH guidelines and all experiments were performed under
1117 protocols approved by the University of Colorado Denver Institutional Animal Care and Use
1118 Committee (IACUC).

1119 For KU1919-GC xenografts, cells that had been stably transduced with non-targeting control
1120 (shCtrl1, SHC002) and NPEPPS (shN39, TRCN0000073839) shRNA constructs. Mice were
1121 divided into groups of 22 and 23 for the non-targeting control and NPEPPS shRNA constructs
1122 respectively. Mice were injected with 4e6 cells in phenol red- and serum-free RPMI mixed with
1123 equal volume Matrigel Matrix (Corning) to total 100 μ l volume. Tumors were allowed to engraft
1124 for 9 days following injection and mice were randomized based on tumor volume within each
1125 shRNA condition into groups of 11 or 12 to be treated with combination gemcitabine plus
1126 cisplatin or DPBS. Treatment was initiated 13 days post-inoculation with dosing adjusted based
1127 on individual mouse weight.

1128 Cisplatin (Sigma) and gemcitabine hydrochloride (BOC Sciences) were both resuspended in
1129 0.9% saline and stored protected from light at -80°C as individual aliquots. Prior to treatment
1130 fresh aliquots of gemcitabine and cisplatin were thawed and diluted to their final concentration
1131 with 1X DPBS (Gibco). Mice were treated three times weekly on a Monday, Wednesday and
1132 Friday schedule for four weeks total. All mice in the gemcitabine plus cisplatin treated groups
1133 were given 50mg/kg gemcitabine and 2mg/kg cisplatin that were mixed and administered as a
1134 single intraperitoneal injection, while control mice were administered an equivalent volume of
1135 DPBS.

1136 Mouse health was monitored daily and all tumor volume measurements and weights were
1137 measured 3x weekly schedule. Tumor volume was calculated using the formula $(L \times W^2)/2$, for
1138 which L is the length of the long axis and W is the width of the axis perpendicular to the long
1139 axis measurement. All measurements were performed using digital calipers. Animal were
1140 humanely euthanized with CO₂ followed by cervical dislocation when tumors reached a
1141 predetermined endpoint of 2cm³ or when weight loss exceeded 15% body weight. Mice that
1142 were removed from study due to weight loss were censored in the survival analyses.

1143

1144 Linear mixed-effects model of tumor growth

1145 Linear mixed-effects models were used to model longitudinal observations of xenograft tumor
 1146 growth volumes normalized by their corresponding baseline volume. Mixed-effects models from
 1147 the R-package *lme4* (Bates et al., 2015) and Satterthwaite's approximation for degrees of
 1148 freedom for the fixed effects from *lmerTest* (Kuznetsova et al., 2017) were used for model fitting
 1149 and inspection in the R statistical software (4.0.3). Volume changes compared to baseline were
 1150 \log_2 -transformed. The final model was structured as:

$$1151 \log_2 \left(\frac{y_{i,t}}{y_{i,:}} \right) = \beta_0 + \beta_1 x_{i,t} + \beta_2 x_{i,t}^2 + \beta_3 x_{i,t} KD_i + \beta_4 x_{i,t} GC_i + \beta_5 x_{i,t} KD_i GC_i + \gamma_{0,i} + \gamma_{1,i} x_{i,t} + \varepsilon_{i,t}$$

1152 where β is the fixed effects capturing population-level trends, γ is the normally distributed
 1153 random effects capturing individual-level variation, ε is the i.i.d. normally distributed residual
 1154 term, i is the unique individual identifier, t notes the time points, $x_{i,t} \in$
 1155 $\{2, 4, 5, 7, 9, 11, 14, 16, 18, 21, 23, 25, 28\}$ depicted days since initiating interventions, $y_{i,:}$ is tumor
 1156 volume at baseline prior to treatments upon randomization, and $y_{i,t}$ were the observed tumor
 1157 volumes over the treatment period measured in mm^3 . The model was fit using Restricted
 1158 Maximum Likelihood and built iteratively until the underlying model assumptions and model
 1159 convergence criteria were met. To this end, a quadratic growth term (β_2) was added on top of
 1160 the linear growth term (β_1) and intercept (β_0), allowing slightly non-linear relative growth patterns
 1161 to be captured by the otherwise linear model. Binary indicators $KD_i \in \{0,1\}$ and $GC_i \in \{0,1\}$ were
 1162 used to model knockdown of NPEPPS, GemCis treatment, or the combination. The
 1163 corresponding model terms were captured in β_3 , β_4 and β_5 , respectively. Finally, the model
 1164 allows for individual-specific random effects for intercept ($\gamma_{0,i}$) and linear growth slope ($\gamma_{1,i}$).
 1165 Shapiro-Wilk test was used to examine the underlying normality assumption for $\gamma_{0,i}$ and $\gamma_{1,i}$ with
 1166 $p=0.1373$ and $p=8901$, respectively, indicating that these random effects followed underlying
 1167 assumptions of normality. After inspection of the residual plots (**Figure S9B**), this final model
 1168 was deemed suitable for population-level statistical inference via the fixed effects. This
 1169 population-level model fits are visualized in **Figure S9A**. These population-level estimates are
 1170 as follows:
 1171

Fixed effect	Estimate	Std. error	df	t	p-val
β_0 (intercept)	0.05054	0.08422	54.28	0.600	0.55091
β_1 (linear slope)	0.1236	0.01493	65.52	8.276	8.92e-12 ***
β_2 (quadratic slope)	0.00308	0.0002242	389	13.740	< 2e-16 ***
β_3 (knockdown)	-0.0605	0.01821	44.97	-3.322	0.00178 **
β_4 (GC)	-0.1063	0.01821	44.97	-5.837	5.49e-07 ***
β_5 (knockdown + GC)	-0.1233	0.01791	45.28	-6.884	1.47e-08 ***

1172

1173 Survival analyses from TCGA

1174 Copy number and gene expression data for patients with muscle-invasive bladder cancer in the
 1175 TCGA cohort (PanCancer Atlas) were downloaded from cBioPortal (Cerami et al., 2012; Gao et
 1176 al., 2013). Patient survival and platinum-based treatment annotation was from our previous work
 1177 (Goodspeed et al., 2019). Patients were separated into treatment groups, platinum-based
 1178 treatment (n = 87) or unrecorded treatment (n = 204), and then stratified based on copy number
 1179 gain or amplification, or mRNA upregulation (z-score > 1) of LRR8A or LRR8D. The Logrank
 1180 test was used to test the difference in overall survival between the stratified patient groups.

1181 **Tumor-derived Organoids**

1182 ***Culture of the organoids***

1183 Human bladder tissue was obtained from the Erasmus MC Bladder Cancer Center, Rotterdam,
1184 the Netherlands. Bladder tumor-derived organoids from biopsies obtained through TURBT or
1185 cystectomy were isolated and cultured using a method based on (Mullenders et al., 2019) with
1186 modifications (Akbarzadeh/Scholtes et al. in prep). Briefly, Bladder tissues were washed with
1187 Advanced DMEM/F12 (Gibco) supplemented with 10mM HEPES (Gibco), 1% GlutaMax (Gibco)
1188 and 100 µg/ml primocin (InvivoGen), henceforth Ad+++. Tissue was minced and incubated at
1189 37°C with the digestion solution (collagenase 2.5mg/ml in EBSS) and isolated cells were passed
1190 through 70µM strainer (Falcon), washed with Ad+++ and seeded in 50 µl drops of BME (R&D
1191 system) containing 10000-15000 cells in 24 well suspension plates (Greiner). Bladder tumor
1192 organoids were cultured in a culture medium containing Ad+++ supplemented with 1 × B-27
1193 (Gibco), 1.25 mM N-acetylcysteine (Sigma), 10 mM nicotinamide, 20µM TGFβ receptor inhibitor
1194 A83-01, 100ng/ml recombinant human FGF10 (PeproTech), 25 ng/ml recombinant human FGF7
1195 (PeproTech), 12.5 ng/ml recombinant human FGF2 (PeproTech), 10µM Y27632 Rho Kinase
1196 (ROCK) Inhibitor (Sigma) and conditioned media for recombinant Rspodin (2.5% v/v), and
1197 Wnt3A (2.5% v/v). The medium was changed every three days. Organoids were passaged at a
1198 1:3 to 1:6 ratio every 7 days using cell dissociation solution- non enzymatic (Sigma) and plated
1199 in fresh BME matrix droplets.

1200 ***Drug screening***

1201 Organoids were collected 7 days after passaging, passed through a 100µM strainer and 1000
1202 organoids were seeded per well of a 48-well plate in BME matrix droplets. After 24h, cisplatin
1203 (Sigma) resuspended in PBS was added at different concentrations (2, 10, 25, and 50 µM) with
1204 or without tosedostat (20 µM) (Tocris) resuspended in DMSO. All wells were adjusted to contain
1205 less than 0.7% DMSO. Organoids were cultured for the first 6 days in the presence of drugs
1206 followed by drug withdrawal, where organoids were grown in organoid culture media for 10
1207 days. The entire content of the wells in different treatment groups was collected, washed and
1208 reseeded after disaggregation in fresh BME, and cultured for 6 days. Cell viability was assayed
1209 using alamarBlue (Invitrogen) according to the manufacturer's instructions after 6 days of drug
1210 incubation, 10 days of drug withdrawal, and 6 days post reseeded. Viability data was
1211 normalized using organoid wells treated with vehicle control.

1212 ***SNaPshot mutation and microarray analysis***

1213 Tumor, organoid, and matched normal DNA was isolated using with the QIAmp DNA Mini-Kit
1214 (Qiagen) according to the manufacturer's protocol. Presence of hotspot mutations in the *TERT*
1215 promoter sequence chr5:1,295,228C>T, chr5:1,295,248G>A and chr5:1,295,250C>T
1216 [GRCh37/hg19]), *FGFR3* (R248Q/E, S249C, G372C, Y375C, A393E, K652E/M) and *PIK3CA*
1217 (E542K, E545G/K and H1047R) were assessed on tumor, normal and organoid DNA by
1218 SNaPshot mutation analysis with the same methods as previously described (Allory et al., 2014;
1219 Hurst et al., 2009; Junker et al., 2008). Copy number aberration analysis was performed using
1220 single-nucleotide polymorphism (SNP) microarrays (Infinium Global Screening Array (GSA) V3,
1221 Illumina) on primary tumor DNA, matched DNA collected from non-tumor urothelium plus
1222 stromal tissue from the same sample but from a distant location from the tumor, and organoid
1223 DNA using standard protocols. SNP data (log-R ratio, B-allele frequency) were visualized to
1224 identify potential CNVs via Biodiscovery Nexus CN7.5. (Biodiscovery) and the GenomeStudio
1225 genotyping module (Illumina).

1226 ***Organoid phenotyping and tumor histology***

1227 Tissue processing and H&E staining was performed using standard procedures. For

1228 hematoxylin-eosin (H&E) staining of organoids, wells of BME-embedded organoids were fixated
1229 with 4% formalin (Sigma) and 0.15% glutaraldehyde (produced in-house) at room temperature
1230 for 2 hours. Fixated BME and organoids were washed with PBS and engulfed in 2.5% Low-
1231 Melting Agarose (Sigma) prior to paraffin embedding. H&E staining was performed on 4 μ M
1232 paraffin sections of both tumor and organoid tissue. Stained whole-slides, as well as prior 3D
1233 organoid cultures were imaged by bright-field microscopy (Olympus IX70).

1234

1235 **Resource Availability**

1236 ***Lead Contact***

1237 Further information and requests for resources and reagents should be directed to and will be
1238 fulfilled by the Lead Contact, James C Costello (james.costello@cuanschutz.edu)
1239

1240 ***Materials Availability***

1241 All unique/stable reagents generated in this study are available from the Lead Contact with a
1242 completed Materials Transfer Agreement
1243

1244 ***Data and code availability***

1245 The mass spectrometry proteomics data have been deposited to the ProteomeXchange
1246 Consortium via the PRIDE (Perez-Riverol et al., 2019) partner repository with the dataset
1247 identifier PXD024742. The whole exome sequencing data have been deposited in the
1248 BioProject database with project identifier PRJNA714778. The RNA sequencing data have been
1249 deposited in the GEO database with dataset identifier (submission in progress). The CRISPR
1250 screen sequencing data have been deposited in the GEO databased with dataset identifier
1251 (submission in progress). The copy number data have been deposited in the ArrayExpress
1252 database with identified (submission in progress).
1253

1254 All data processing pipelines are described in the STAR Methods and corresponding software
1255 packages are listed in the Key Resource Table.
1256

1257 **Acknowledgements**

1258

1259 We would like to thank Megan Tu, Colin Sempeck, Ana Chauca-Diaz, Jason Duex, and Charles
1260 Owens for their help throughout this project. We would also like to thank Dania Manalo-Mae and
1261 the Cedars-Sinai Proteomics and Metabolomics Core facility for technical handling of the
1262 proteomic experiments. This work was generously supported by the Anschutz Foundation to
1263 J.C.C., CA180175 to D.T., FICAN Cancer Researcher by the Finnish Cancer Institute to T.D.L.,
1264 Erasmus MC mRACE grant 111296 to T.M. and T.Z., Erasmus MC fellowship project 107088 to
1265 T.Z., and training grants GM007635 and GM008497 supported R.T.J. This work utilized the
1266 Functional Genomics Facility, Biostatistics and Bioinformatics Shared Resource, Genomics
1267 Shared Resource, and Flow Cytometry Shared Resource supported by CA046934.

1268

1269 **Author Contributions**

1270

1271 Conceptualization: R.T.J., T.M., T.Z., D.T., J.C.C.

1272 Methodology: R.T.J., A.G., M.S., H.V., A.J., T.D.L., M.A., E.C., S.P., T.M., T.Z., D.T., J.C.C.

1273 Software: A.G., T.D.L., M.J., R.L., J.C.C.

1274 Validation: R.T.J., A.G., M.S., A.J., C.T., M.V.O., S.A., S.M., T.Z.

1275 Formal Analysis: R.T.J., A.G., M.S., H.V., T.D.L., M.V.O., M.J., E.C., S.P., T.Z., D.T., J.C.C.

1276 Investigation: R.T.J., M.A., M.S., H.V., A.J., C.T., M.V.O., S.A., S.M., E.C., S.P., T.Z., J.C.C.

1277 Resources: A.J., C.T., E.C., R.L., T.Z.

1278 Data Curation: R.T.J., A.G., A.J., T.D.L., M.J., R.L., J.C.C.

1279 Writing – Original Draft: R.T.J., A.G., D.T., J.C.C.

1280 Writing – Review & Editing: R.T.J., A.G., M.A., M.S., H.V., M.V.O., M.J., T.D.L., E.C., S.P., T.M.,
1281 T.Z., D.T., J.C.C.

1282 Visualization: R.T.J., A.G., M.A., M.S., M.V.O., T.D.L., E.C., T.Z., D.T., J.C.C.

1283 Supervision: R.L., T.M., D.T., T.Z., J.C.C.

1284 Project Administration: R.T.J., A.J., T.M., T.Z., D.T., J.C.C.

1285 Funding Acquisition: T.M., T.Z., D.T., J.C.C.

1286

1287 **Declaration of Interests**

1288 A provisional patent 63/153,519 has been filed on the subject matter of this work. J.C.C. is co-
1289 founder of PrecisionProfile. All other authors declare no competing interests.

1290

1291 **References**

- 1292 1000 Genomes Project Consortium, Auton, A., Brooks, L.D., Durbin, R.M., Garrison, E.P., Kang,
1293 H.M., Korbelt, J.O., Marchini, J.L., McCarthy, S., McVean, G.A., et al. (2015). A global reference
1294 for human genetic variation. *Nature* 526, 68–74.
- 1295 Agarwal, N., Dancik, G.M., Goodspeed, A., Costello, J.C., Owens, C., Duex, J.E., and Theodorescu,
1296 D. (2016). GON4L Drives Cancer Growth through a YY1-Androgen Receptor-CD24 Axis. *Cancer*
1297 *Res.* 76, 5175–5185.
- 1298 Allory, Y., Beukers, W., Sagraera, A., Flández, M., Marqués, M., Márquez, M., van der Keur, K.A.,
1299 Dyrskjot, L., Lurkin, I., Vermeij, M., et al. (2014). Telomerase reverse transcriptase promoter
1300 mutations in bladder cancer: high frequency across stages, detection in urine, and lack of
1301 association with outcome. *Eur. Urol.* 65, 360–366.
- 1302 Balar, A.V., Galsky, M.D., Rosenberg, J.E., Powles, T., Petrylak, D.P., Bellmunt, J., Loriot, Y.,
1303 Necchi, A., Hoffman-Censits, J., Perez-Gracia, J.L., et al. (2017). Atezolizumab as first-line
1304 treatment in cisplatin-ineligible patients with locally advanced and metastatic urothelial
1305 carcinoma: a single-arm, multicentre, phase 2 trial. *Lancet Lond. Engl.* 389, 67–76.
- 1306 Bates, D., Mächler, M., Bolker, B., and Walker, S. (2015). Fitting Linear Mixed-Effects Models
1307 Using lme4. *J. Stat. Softw.* 67, 1–48.
- 1308 Behan, F.M., Iorio, F., Picco, G., Gonçalves, E., Beaver, C.M., Migliardi, G., Santos, R., Rao, Y.,
1309 Sassi, F., Pinnelli, M., et al. (2019). Prioritization of cancer therapeutic targets using CRISPR–
1310 Cas9 screens. *Nature* 568, 511–516.
- 1311 Benjamin, D., Sato, T., Cibulskis, K., Getz, G., Stewart, C., and Lichtenstein, L. (2019). Calling
1312 Somatic SNVs and Indels with Mutect2. *BioRxiv* 861054.
- 1313 Bepler, G., Kusmartseva, I., Sharma, S., Gautam, A., Cantor, A., Sharma, A., and Simon, G.
1314 (2006). RRM1 modulated in vitro and in vivo efficacy of gemcitabine and platinum in non-small-
1315 cell lung cancer. *J. Clin. Oncol. Off. J. Am. Soc. Clin. Oncol.* 24, 4731–4737.
- 1316 Bergman, A.M., Eijk, P.P., Ruiz van Haperen, V.W.T., Smid, K., Veerman, G., Hubeek, I., van den
1317 Ijssel, P., Ylstra, B., and Peters, G.J. (2005). In vivo induction of resistance to gemcitabine results
1318 in increased expression of ribonucleotide reductase subunit M1 as the major determinant.
1319 *Cancer Res.* 65, 9510–9516.
- 1320 Berle, M., Ghila, L., Vethe, H., Chaudhry, A., Garberg, H., Beisland, C., Haaland, Ø.A., Oveland,
1321 E., Halvorsen, O.J., Davidsson, T., et al. (2018). Novel protein signatures suggest progression to
1322 muscular invasiveness in bladder cancer. *PLoS One* 13, e0206475.
- 1323 Bray, F., Ferlay, J., Soerjomataram, I., Siegel, R.L., Torre, L.A., and Jemal, A. (2018). Global cancer
1324 statistics 2018: GLOBOCAN estimates of incidence and mortality worldwide for 36 cancers in
1325 185 countries. *CA. Cancer J. Clin.* 68, 394–424.

- 1326 Cerami, E., Gao, J., Dogrusoz, U., Gross, B.E., Sumer, S.O., Aksoy, B.A., Jacobsen, A., Byrne, C.J.,
1327 Heuer, M.L., Larsson, E., et al. (2012). The cBio Cancer Genomics Portal: An Open Platform for
1328 Exploring Multidimensional Cancer Genomics Data. *Cancer Discov.* *2*, 401–404.
- 1329 Chang, Q., Ornatsky, O.I., Koch, C.J., Chaudary, N., Marie-Egyptienne, D.T., Hill, R.P., Tanner,
1330 S.D., and Hedley, D.W. (2015). Single-cell measurement of the uptake, intratumoral distribution
1331 and cell cycle effects of cisplatin using mass cytometry. *Int. J. Cancer* *136*, 1202–1209.
- 1332 Choi, M., Chang, C.-Y., Clough, T., Broudy, D., Killeen, T., MacLean, B., and Vitek, O. (2014).
1333 MSstats: an R package for statistical analysis of quantitative mass spectrometry-based
1334 proteomic experiments. *Bioinforma. Oxf. Engl.* *30*, 2524–2526.
- 1335 Clasquin, M.F., Melamud, E., and Rabinowitz, J.D. (2012). LC-MS data processing with MAVEN: a
1336 metabolomic analysis and visualization engine. *Curr. Protoc. Bioinforma. Chapter 14*, Unit14.11.
- 1337 Compagnone, M., Cifaldi, L., and Fruci, D. (2019). Regulation of ERAP1 and ERAP2 genes and
1338 their dysfunction in human cancer. *Hum. Immunol.* *80*, 318–324.
- 1339 Constam, D.B., Tobler, A.R., Rensing-Ehl, A., Kemler, I., Hersh, L.B., and Fontana, A. (1995).
1340 Puromycin-sensitive aminopeptidase. Sequence analysis, expression, and functional
1341 characterization. *J. Biol. Chem.* *270*, 26931–26939.
- 1342 Cortes, J., Feldman, E., Yee, K., Rizzieri, D., Advani, A.S., Charman, A., Spruyt, R., Toal, M., and
1343 Kantarjian, H. (2013). Two dosing regimens of tosedostat in elderly patients with relapsed or
1344 refractory acute myeloid leukaemia (OPAL): a randomised open-label phase 2 study. *Lancet*
1345 *Oncol.* *14*, 354–362.
- 1346 Cowley, G.S., Weir, B.A., Vazquez, F., Tamayo, P., Scott, J.A., Rusin, S., East-Seletsky, A., Ali, L.D.,
1347 Gerath, W.F., Pantel, S.E., et al. (2014). Parallel genome-scale loss of function screens in 216
1348 cancer cell lines for the identification of context-specific genetic dependencies. *Sci. Data* *1*,
1349 140035.
- 1350 Dempster, J.M., Krill-Burger, J., Warren, A., McFarland, J.M., Golub, T.R., and Tsherniak, A.
1351 (2020). Gene expression has more power for predicting in vitro cancer cell vulnerabilities than
1352 genomics. *BioRxiv* 2020.02.21.959627.
- 1353 Dilruba, S., and Kalayda, G.V. (2016). Platinum-based drugs: past, present and future. *Cancer*
1354 *Chemother. Pharmacol.* *77*, 1103–1124.
- 1355 Dobin, A., Davis, C.A., Schlesinger, F., Drenkow, J., Zaleski, C., Jha, S., Batut, P., Chaisson, M.,
1356 and Gingeras, T.R. (2013). STAR: ultrafast universal RNA-seq aligner. *Bioinforma. Oxf. Engl.* *29*,
1357 15–21.
- 1358 Doench, J.G., Fusi, N., Sullender, M., Hegde, M., Vaimberg, E.W., Donovan, K.F., Smith, I.,
1359 Tothova, Z., Wilen, C., Orchard, R., et al. (2016). Optimized sgRNA design to maximize activity
1360 and minimize off-target effects of CRISPR-Cas9. *Nat. Biotechnol.* *34*, 184–191.

- 1361 Drayton, R.M., and Catto, J.W. (2012). Molecular mechanisms of cisplatin resistance in bladder
1362 cancer. *Expert Rev. Anticancer Ther.* *12*, 271–281.
- 1363 Drinkwater, N., Lee, J., Yang, W., Malcolm, T.R., and McGowan, S. (2017). M1 aminopeptidases
1364 as drug targets: broad applications or therapeutic niche? *FEBS J.* *284*, 1473–1488.
- 1365 Faust, G.G., and Hall, I.M. (2014). SAMBLASTER: fast duplicate marking and structural variant
1366 read extraction. *Bioinforma. Oxf. Engl.* *30*, 2503–2505.
- 1367 FlowJo (2019). FlowJo Software (for Mac) (Becton, Dickenson and Company).
- 1368 Galluzzi, L., Senovilla, L., Vitale, I., Michels, J., Martins, I., Kepp, O., Castedo, M., and Kroemer,
1369 G. (2012). Molecular mechanisms of cisplatin resistance. *Oncogene* *31*, 1869–1883.
- 1370 Galsky, M.D., Pal, S.K., Lin, S.-W., Ogale, S., Zivkovic, M., Simpson, J., Derleth, C., Schiff, C., and
1371 Sonpavde, G. (2018). Real-World Effectiveness of Chemotherapy in Elderly Patients With
1372 Metastatic Bladder Cancer in the United States. *Bladder Cancer Amst. Neth.* *4*, 227–238.
- 1373 Galsky, M.D., Arija, J.Á.A., Bamias, A., Davis, I.D., De Santis, M., Kikuchi, E., Garcia-Del-Muro, X.,
1374 De Giorgi, U., Mencinger, M., Izumi, K., et al. (2020). Atezolizumab with or without
1375 chemotherapy in metastatic urothelial cancer (IMvigor130): a multicentre, randomised,
1376 placebo-controlled phase 3 trial. *Lancet Lond. Engl.* *395*, 1547–1557.
- 1377 Gao, J., Aksoy, B.A., Dogrusoz, U., Dresdner, G., Gross, B., Sumer, S.O., Sun, Y., Jacobsen, A.,
1378 Sinha, R., Larsson, E., et al. (2013). Integrative Analysis of Complex Cancer Genomics and Clinical
1379 Profiles Using the cBioPortal. *Sci. Signal.* *6*, pl1–pl1.
- 1380 Gehrke, S., Rice, S., Stefanoni, D., Wilkerson, R.B., Nemkov, T., Reisz, J.A., Hansen, K.C., Lucas,
1381 A., Cabrales, P., Drew, K., et al. (2019). Red Blood Cell Metabolic Responses to Torpor and
1382 Arousal in the Hibernator Arctic Ground Squirrel. *J. Proteome Res.* *18*, 1827–1841.
- 1383 Goodspeed, A., Jean, A., and Costello, J.C. (2019). A Whole-genome CRISPR Screen Identifies a
1384 Role of MSH2 in Cisplatin-mediated Cell Death in Muscle-invasive Bladder Cancer. *Eur. Urol.* *75*,
1385 242–250.
- 1386 Grossman, H.B., Natale, R.B., Tangen, C.M., Speights, V.O., Vogelzang, N.J., Trump, D.L., White,
1387 R.W. deVere, Sarosdy, M.F., Wood, D.P., Raghavan, D., et al. (2003). Neoadjuvant
1388 Chemotherapy plus Cystectomy Compared with Cystectomy Alone for Locally Advanced Bladder
1389 Cancer. *N. Engl. J. Med.* *349*, 859–866.
- 1390 Gu, Z., Eils, R., and Schlesner, M. (2016). Complex heatmaps reveal patterns and correlations in
1391 multidimensional genomic data. *Bioinformatics* *32*, 2847–2849.
- 1392 van Herpen, C.M.L., Eskens, F. a. L.M., de Jonge, M., Desar, I., Hooftman, L., Bone, E.A., Timmer-
1393 Bonte, J.N.H., and Verweij, J. (2010). A Phase Ib dose-escalation study to evaluate safety and

- 1394 tolerability of the addition of the aminopeptidase inhibitor tosedostat (CHR-2797) to paclitaxel
1395 in patients with advanced solid tumours. *Br. J. Cancer* *103*, 1362–1368.
- 1396 Hitzerd, S.M., Verbrugge, S.E., Ossenkoppele, G., Jansen, G., and Peters, G.J. (2014). Positioning
1397 of aminopeptidase inhibitors in next generation cancer therapy. *Amino Acids* *46*, 793–808.
- 1398 Huang, A., Garraway, L.A., Ashworth, A., and Weber, B. (2020). Synthetic lethality as an engine
1399 for cancer drug target discovery. *Nat. Rev. Drug Discov.* *19*, 23–38.
- 1400 Huber, W., von Heydebreck, A., Sülthmann, H., Poustka, A., and Vingron, M. (2002). Variance
1401 stabilization applied to microarray data calibration and to the quantification of differential
1402 expression. *Bioinforma. Oxf. Engl.* *18 Suppl 1*, S96-104.
- 1403 Hurst, C.D., Zuiverloon, T.C.M., Hafner, C., Zwarthoff, E.C., and Knowles, M.A. (2009). A
1404 SNaPshot assay for the rapid and simple detection of four common hotspot codon mutations in
1405 the PIK3CA gene. *BMC Res. Notes* *2*, 66.
- 1406 Huttlin, E.L., Bruckner, R.J., Navarrete-Perea, J., Cannon, J.R., Baltier, K., Gebreab, F., Gygi, M.P.,
1407 Thornock, A., Zarraga, G., Tam, S., et al. (2020). Dual Proteome-scale Networks Reveal Cell-
1408 specific Remodeling of the Human Interactome. *BioRxiv* 2020.01.19.905109.
- 1409 Imkeller, K., Ambrosi, G., Boutros, M., and Huber, W. (2020). gscreend: modelling asymmetric
1410 count ratios in CRISPR screens to decrease experiment size and improve phenotype detection.
1411 *Genome Biol.* *21*, 53.
- 1412 Jackson, P.S., and Strange, K. (1993). Volume-sensitive anion channels mediate swelling-
1413 activated inositol and taurine efflux. *Am. J. Physiol.* *265*, C1489-1500.
- 1414 Jordheim, L.P., Sève, P., Trédan, O., and Dumontet, C. (2011). The ribonucleotide reductase
1415 large subunit (RRM1) as a predictive factor in patients with cancer. *Lancet Oncol.* *12*, 693–702.
- 1416 Jost, M., and Weissman, J.S. (2018). CRISPR Approaches to Small Molecule Target Identification.
1417 *ACS Chem. Biol.* *13*, 366–375.
- 1418 Joung, J., Konermann, S., Gootenberg, J.S., Abudayyeh, O.O., Platt, R.J., Brigham, M.D., Sanjana,
1419 N.E., and Zhang, F. (2017). Genome-scale CRISPR-Cas9 knockout and transcriptional activation
1420 screening. *Nat. Protoc.* *12*, 828–863.
- 1421 Junker, K., van Oers, J.M.M., Zwarthoff, E.C., Kania, I., Schubert, J., and Hartmann, A. (2008).
1422 Fibroblast growth factor receptor 3 mutations in bladder tumors correlate with low frequency
1423 of chromosome alterations. *Neoplasia N. Y. N* *10*, 1–7.
- 1424 Karczewski, K.J., Francioli, L.C., Tiao, G., Cummings, B.B., Alföldi, J., Wang, Q., Collins, R.L.,
1425 Laricchia, K.M., Ganna, A., Birnbaum, D.P., et al. (2020). The mutational constraint spectrum
1426 quantified from variation in 141,456 humans. *Nature* *581*, 434–443.

- 1427 Karsten, S.L., Sang, T.-K., Gehman, L.T., Chatterjee, S., Liu, J., Lawless, G.M., Sengupta, S., Berry,
1428 R.W., Pomakian, J., Oh, H.S., et al. (2006). A genomic screen for modifiers of tauopathy
1429 identifies puromycin-sensitive aminopeptidase as an inhibitor of tau-induced
1430 neurodegeneration. *Neuron* 51, 549–560.
- 1431 Kasuya, G., Nakane, T., Yokoyama, T., Jia, Y., Inoue, M., Watanabe, K., Nakamura, R., Nishizawa,
1432 T., Kusakizako, T., Tsutsumi, A., et al. (2018). Cryo-EM structures of the human volume-
1433 regulated anion channel LRRC8. *Nat. Struct. Mol. Biol.* 25, 797–804.
- 1434 Korotkevich, G., Sukhov, V., and Sergushichev, A. (2019). Fast gene set enrichment analysis.
1435 BioRxiv 060012.
- 1436 Krige, D., Needham, L.A., Bawden, L.J., Flores, N., Farmer, H., Miles, L.E.C., Stone, E., Callaghan,
1437 J., Chandler, S., Clark, V.L., et al. (2008). CHR-2797: an antiproliferative aminopeptidase
1438 inhibitor that leads to amino acid deprivation in human leukemic cells. *Cancer Res.* 68, 6669–
1439 6679.
- 1440 Kudo, L.C., Parfenova, L., Ren, G., Vi, N., Hui, M., Ma, Z., Lau, K., Gray, M., Bardag-Gorce, F.,
1441 Wiedau-Pazos, M., et al. (2011). Puromycin-sensitive aminopeptidase (PSA/NPEPPS) impedes
1442 development of neuropathology in hPSA/TAU(P301L) double-transgenic mice. *Hum. Mol.*
1443 *Genet.* 20, 1820–1833.
- 1444 Kuznetsova, A., Brockhoff, P.B., and Christensen, R.H.B. (2017). lmerTest Package: Tests in
1445 Linear Mixed Effects Models. *J. Stat. Softw.* 82, 1–26.
- 1446 Landrum, M.J., Lee, J.M., Benson, M., Brown, G.R., Chao, C., Chitipiralla, S., Gu, B., Hart, J.,
1447 Hoffman, D., Jang, W., et al. (2018). ClinVar: improving access to variant interpretations and
1448 supporting evidence. *Nucleic Acids Res.* 46, D1062–D1067.
- 1449 Laver, T.W., Franco, E.D., Johnson, M.B., Patel, K., Ellard, S., Weedon, M.N., Flanagan, S.E., and
1450 Wakeling, M.N. (2019). SavvyCNV: genome-wide CNV calling from off-target reads. BioRxiv
1451 617605.
- 1452 Li, H. (2013). Aligning sequence reads, clone sequences and assembly contigs with BWA-MEM.
1453 ArXiv13033997 Q-Bio.
- 1454 Li, H., Handsaker, B., Wysoker, A., Fennell, T., Ruan, J., Homer, N., Marth, G., Abecasis, G., and
1455 Durbin, R. (2009). The Sequence Alignment/Map format and SAMtools. *Bioinformatics* 25,
1456 2078–2079.
- 1457 Liberzon, A., Subramanian, A., Pinchback, R., Thorvaldsdóttir, H., Tamayo, P., and Mesirov, J.P.
1458 (2011). Molecular signatures database (MSigDB) 3.0. *Bioinformatics* 27, 1739–1740.
- 1459 Lim, Y.W., Chen-Harris, H., Mayba, O., Lianoglou, S., Wuster, A., Bhangale, T., Khan, Z.,
1460 Mariathasan, S., Daemen, A., Reeder, J., et al. (2018). Germline genetic polymorphisms

- 1461 influence tumor gene expression and immune cell infiltration. *Proc. Natl. Acad. Sci.* *115*,
1462 E11701–E11710.
- 1463 Love, M.I., Huber, W., and Anders, S. (2014). Moderated estimation of fold change and
1464 dispersion for RNA-seq data with DESeq2. *Genome Biol.* *15*, 550.
- 1465 Löwenberg, B., Morgan, G., Ossenkoppele, G.J., Burnett, A.K., Zachée, P., Dührsen, U., Dierickx,
1466 D., Müller-Tidow, C., Sonneveld, P., Krug, U., et al. (2010). Phase I/II clinical study of Tosedostat,
1467 an inhibitor of aminopeptidases, in patients with acute myeloid leukemia and myelodysplasia. *J.*
1468 *Clin. Oncol. Off. J. Am. Soc. Clin. Oncol.* *28*, 4333–4338.
- 1469 Mawad, R., Becker, P.S., Hendrie, P., Scott, B., Wood, B.L., Dean, C., Sandhu, V., Deeg, H.J.,
1470 Walter, R., Wang, L., et al. (2016). Phase II study of tosedostat with cytarabine or decitabine in
1471 newly diagnosed older patients with acute myeloid leukaemia or high-risk MDS. *Br. J. Haematol.*
1472 *172*, 238–245.
- 1473 McDonald, E.R., de Weck, A., Schlabach, M.R., Billy, E., Mavrakis, K.J., Hoffman, G.R., Belur, D.,
1474 Castelletti, D., Frias, E., Gampa, K., et al. (2017). Project DRIVE: A Compendium of Cancer
1475 Dependencies and Synthetic Lethal Relationships Uncovered by Large-Scale, Deep RNAi
1476 Screening. *Cell* *170*, 577-592.e10.
- 1477 Menzies, F.M., Hourez, R., Imarisio, S., Raspe, M., Sadiq, O., Chandraratna, D., O’Kane, C., Rock,
1478 K.L., Reits, E., Goldberg, A.L., et al. (2010). Puromycin-sensitive aminopeptidase protects against
1479 aggregation-prone proteins via autophagy. *Hum. Mol. Genet.* *19*, 4573–4586.
- 1480 Mills, R.E., Pittard, W.S., Mullaney, J.M., Farooq, U., Creasy, T.H., Mahurkar, A.A., Kemeza, D.M.,
1481 Strassler, D.S., Ponting, C.P., Webber, C., et al. (2011). Natural genetic variation caused by small
1482 insertions and deletions in the human genome. *Genome Res.* *21*, 830–839.
- 1483 Mullenders, J., de Jongh, E., Brousalı, A., Roosen, M., Blom, J.P.A., Begthel, H., Korving, J.,
1484 Jonges, T., Kranenburg, O., Meijer, R., et al. (2019). Mouse and human urothelial cancer
1485 organoids: A tool for bladder cancer research. *Proc. Natl. Acad. Sci. U. S. A.* *116*, 4567–4574.
- 1486 Nadal, R., and Bellmunt, J. (2019). Management of metastatic bladder cancer. *Cancer Treat.*
1487 *Rev.* *76*, 10–21.
- 1488 Nemkov, T., D’Alessandro, A., and Hansen, K.C. (2015). Three-minute method for amino acid
1489 analysis by UHPLC and high-resolution quadrupole orbitrap mass spectrometry. *Amino Acids* *47*,
1490 2345–2357.
- 1491 Nemkov, T., Reisz, J.A., Gehrke, S., Hansen, K.C., and D’Alessandro, A. (2019). High-Throughput
1492 Metabolomics: Isocratic and Gradient Mass Spectrometry-Based Methods. *Methods Mol. Biol.*
1493 Clifton NJ *1978*, 13–26.

- 1494 Okonechnikov, K., Conesa, A., and García-Alcalde, F. (2016). Qualimap 2: advanced multi-
1495 sample quality control for high-throughput sequencing data. *Bioinforma. Oxf. Engl.* *32*, 292–
1496 294.
- 1497 Olivieri, M., Cho, T., Álvarez-Quilón, A., Li, K., Schellenberg, M.J., Zimmermann, M., Hustedt, N.,
1498 Rossi, S.E., Adam, S., Melo, H., et al. (2020). A Genetic Map of the Response to DNA Damage in
1499 Human Cells. *Cell* *182*, 481-496.e21.
- 1500 Osada, T., Ikegami, S., Takiguchi-Hayashi, K., Yamazaki, Y., Katoh-Fukui, Y., Higashinakagawa, T.,
1501 Sakaki, Y., and Takeuchi, T. (1999). Increased anxiety and impaired pain response in puromycin-
1502 sensitive aminopeptidase gene-deficient mice obtained by a mouse gene-trap method. *J.*
1503 *Neurosci. Off. J. Soc. Neurosci.* *19*, 6068–6078.
- 1504 Parker, S.J., Rost, H., Rosenberger, G., Collins, B.C., Malmström, L., Amodei, D., Venkatraman,
1505 V., Raedschelders, K., Van Eyk, J.E., and Aebersold, R. (2015). Identification of a Set of
1506 Conserved Eukaryotic Internal Retention Time Standards for Data-independent Acquisition
1507 Mass Spectrometry. *Mol. Cell. Proteomics MCP* *14*, 2800–2813.
- 1508 Parker, S.J., Venkatraman, V., and Van Eyk, J.E. (2016). Effect of peptide assay library size and
1509 composition in targeted data-independent acquisition-MS analyses. *Proteomics* *16*, 2221–2237.
- 1510 Patel, V.G., Oh, W.K., and Galsky, M.D. (2020). Treatment of muscle-invasive and advanced
1511 bladder cancer in 2020. *CA. Cancer J. Clin.*
- 1512 Perez-Riverol, Y., Csordas, A., Bai, J., Bernal-Llinares, M., Hewapathirana, S., Kundu, D.J.,
1513 Inuganti, A., Griss, J., Mayer, G., Eisenacher, M., et al. (2019). The PRIDE database and related
1514 tools and resources in 2019: improving support for quantification data. *Nucleic Acids Res.* *47*,
1515 D442–D450.
- 1516 Planells-Cases, R., Lutter, D., Guyader, C., Gerhards, N.M., Ullrich, F., Elger, D.A.,
1517 Kucukosmanoglu, A., Xu, G., Voss, F.K., Reincke, S.M., et al. (2015). Subunit composition of
1518 VRAC channels determines substrate specificity and cellular resistance to Pt-based anti-cancer
1519 drugs. *EMBO J.* *34*, 2993–3008.
- 1520 Qiu, Z., Dubin, A.E., Mathur, J., Tu, B., Reddy, K., Miraglia, L.J., Reinhardt, J., Orth, A.P., and
1521 Patapoutian, A. (2014). SWELL1, a plasma membrane protein, is an essential component of
1522 volume-regulated anion channel. *Cell* *157*, 447–458.
- 1523 Reid, A.H.M., Protheroe, A., Attard, G., Hayward, N., Vidal, L., Spicer, J., Shaw, H.M., Bone, E.A.,
1524 Carter, J., Hooftman, L., et al. (2009). A First-in-Man Phase I and Pharmacokinetic Study on CHR-
1525 2797 (Tosedostat), an Inhibitor of M1 Aminopeptidases, in Patients with Advanced Solid
1526 Tumors. *Clin. Cancer Res.* *15*, 4978–4985.
- 1527 Ritchie, M.E., Phipson, B., Wu, D., Hu, Y., Law, C.W., Shi, W., and Smyth, G.K. (2015). limma
1528 powers differential expression analyses for RNA-sequencing and microarray studies. *Nucleic*
1529 *Acids Res.* *43*, e47.

- 1530 Robertson, A.G., Kim, J., Al-Ahmadie, H., Bellmunt, J., Guo, G., Cherniack, A.D., Hinoue, T., Laird,
1531 P.W., Hoadley, K.A., Akbani, R., et al. (2017). Comprehensive Molecular Characterization of
1532 Muscle-Invasive Bladder Cancer. *Cell* *171*, 540-556.e25.
- 1533 Robinson, A.E., Binek, A., Venkatraman, V., Searle, B.C., Holewinski, R.J., Rosenberger, G.,
1534 Parker, S.J., Basisty, N., Xie, X., Lund, P.J., et al. (2020). Lysine and Arginine Protein Post-
1535 translational Modifications by Enhanced DIA Libraries: Quantification in Murine Liver Disease. *J.*
1536 *Proteome Res.* *19*, 4163–4178.
- 1537 Robinson, M.D., McCarthy, D.J., and Smyth, G.K. (2010). edgeR: a Bioconductor package for
1538 differential expression analysis of digital gene expression data. *Bioinforma. Oxf. Engl.* *26*, 139–
1539 140.
- 1540 Röst, H.L., Rosenberger, G., Navarro, P., Gillet, L., Miladinović, S.M., Schubert, O.T., Wolski, W.,
1541 Collins, B.C., Malmström, J., Malmström, L., et al. (2014). OpenSWATH enables automated,
1542 targeted analysis of data-independent acquisition MS data. *Nat. Biotechnol.* *32*, 219–223.
- 1543 Röst, H.L., Liu, Y., D’Agostino, G., Zanella, M., Navarro, P., Rosenberger, G., Collins, B.C., Gillet,
1544 L., Testa, G., Malmström, L., et al. (2016). TRIC: an automated alignment strategy for
1545 reproducible protein quantification in targeted proteomics. *Nat. Methods* *13*, 777–783.
- 1546 Rottenberg, S., Disler, C., and Perego, P. (2021). The rediscovery of platinum-based cancer
1547 therapy. *Nat. Rev. Cancer* *21*, 37–50.
- 1548 Saric, T., Graef, C.I., and Goldberg, A.L. (2004). Pathway for degradation of peptides generated
1549 by proteasomes: a key role for thimet oligopeptidase and other metallopeptidases. *J. Biol.*
1550 *Chem.* *279*, 46723–46732.
- 1551 Schönlein, C., Löffler, J., and Huber, G. (1994). Purification and characterization of a novel
1552 metalloprotease from human brain with the ability to cleave substrates derived from the N-
1553 terminus of beta-amyloid protein. *Biochem. Biophys. Res. Commun.* *201*, 45–53.
- 1554 Sergushichev, A.A. (2016). An algorithm for fast preranked gene set enrichment analysis using
1555 cumulative statistic calculation. *BioRxiv* 060012.
- 1556 Sherry, S.T., Ward, M.H., Kholodov, M., Baker, J., Phan, L., Smigielski, E.M., and Sirotkin, K.
1557 (2001). dbSNP: the NCBI database of genetic variation. *Nucleic Acids Res.* *29*, 308–311.
- 1558 Sørensen, B.H., Thorsteinsdottir, U.A., and Lambert, I.H. (2014). Acquired cisplatin resistance in
1559 human ovarian A2780 cancer cells correlates with shift in taurine homeostasis and ability to
1560 volume regulate. *Am. J. Physiol.-Cell Physiol.* *307*, C1071–C1080.
- 1561 Sørensen, B.H., Nielsen, D., Thorsteinsdottir, U.A., Hoffmann, E.K., and Lambert, I.H. (2016a).
1562 Downregulation of LRRC8A protects human ovarian and alveolar carcinoma cells against
1563 Cisplatin-induced expression of p53, MDM2, p21Waf1/Cip1, and Caspase-9/-3 activation. *Am. J.*
1564 *Physiol.-Cell Physiol.* *310*, C857–C873.

- 1565 Sørensen, B.H., Dam, C.S., Stürup, S., and Lambert, I.H. (2016b). Dual role of LRRC8A-containing
1566 transporters on cisplatin resistance in human ovarian cancer cells. *J. Inorg. Biochem.* *160*, 287–
1567 295.
- 1568 Syeda, R., Qiu, Z., Dubin, A.E., Murthy, S.E., Florendo, M.N., Mason, D.E., Mathur, J., Cahalan,
1569 S.M., Peters, E.C., Montal, M., et al. (2016). LRRC8 Proteins Form Volume-Regulated Anion
1570 Channels that Sense Ionic Strength. *Cell* *164*, 499–511.
- 1571 Teleman, J., Röst, H.L., Rosenberger, G., Schmitt, U., Malmström, L., Malmström, J., and
1572 Levander, F. (2015). DIANA--algorithmic improvements for analysis of data-independent
1573 acquisition MS data. *Bioinforma. Oxf. Engl.* *31*, 555–562.
- 1574 Towne, C.F., York, I.A., Neijssen, J., Karow, M.L., Murphy, A.J., Valenzuela, D.M., Yancopoulos,
1575 G.D., Neefjes, J.J., and Rock, K.L. (2008). Puromycin-Sensitive Aminopeptidase Limits MHC Class
1576 I Presentation in Dendritic Cells but Does Not Affect CD8 T Cell Responses during Viral
1577 Infections. *J. Immunol.* *180*, 1704–1712.
- 1578 Tsherniak, A., Vazquez, F., Montgomery, P.G., Weir, B.A., Kryukov, G., Cowley, G.S., Gill, S.,
1579 Harrington, W.F., Pantel, S., Krill-Burger, J.M., et al. (2017). Defining a Cancer Dependency Map.
1580 *Cell* *170*, 564-576.e16.
- 1581 Uhlen, M., Zhang, C., Lee, S., Sjöstedt, E., Fagerberg, L., Bidkhori, G., Benfeitas, R., Arif, M., Liu,
1582 Z., Edfors, F., et al. (2017). A pathology atlas of the human cancer transcriptome. *Science* *357*.
- 1583 Vale, C.L. (2005). Neoadjuvant Chemotherapy in Invasive Bladder Cancer: Update of a
1584 Systematic Review and Meta-Analysis of Individual Patient Data: Advanced Bladder Cancer
1585 (ABC) Meta-analysis Collaboration. *Eur. Urol.* *48*, 202–206.
- 1586 Vallo, S., Michaelis, M., Rothweiler, F., Bartsch, G., Gust, K.M., Limbart, D.M., Rödel, F., Wezel,
1587 F., Haferkamp, A., and Cinatl, J. (2015). Drug-Resistant Urothelial Cancer Cell Lines Display
1588 Diverse Sensitivity Profiles to Potential Second-Line Therapeutics. *Transl. Oncol.* *8*, 210–216.
- 1589 Vallo, S., Köpp, R., Michaelis, M., Rothweiler, F., Bartsch, G., Brandt, M.P., Gust, K.M., Wezel, F.,
1590 Blaheta, R.A., Haferkamp, A., et al. (2017). Resistance to nanoparticle albumin-bound paclitaxel
1591 is mediated by ABCB1 in urothelial cancer cells. *Oncol. Lett.* *13*, 4085–4092.
- 1592 Voss, F.K., Ullrich, F., Münch, J., Lazarow, K., Lutter, D., Mah, N., Andrade-Navarro, M.A., von
1593 Kries, J.P., Stauber, T., and Jentsch, T.J. (2014). Identification of LRRC8 heteromers as an
1594 essential component of the volume-regulated anion channel VRAC. *Science* *344*, 634–638.
- 1595 Wang, K., Li, M., and Hakonarson, H. (2010). ANNOVAR: functional annotation of genetic
1596 variants from high-throughput sequencing data. *Nucleic Acids Res.* *38*, e164–e164.
- 1597 Wickham, H. (2009). *Ggplot2: elegant graphics for data analysis* (New York: Springer).

- 1598 Winter, J., Breinig, M., Heigwer, F., Brügemann, D., Leible, S., Pelz, O., Zhan, T., and Boutros, M.
1599 (2016). caRpoools: an R package for exploratory data analysis and documentation of pooled
1600 CRISPR/Cas9 screens. *Bioinforma. Oxf. Engl.* *32*, 632–634.
- 1601 Witjes, J.A., Bruins, H.M., Cathomas, R., Compérat, E.M., Cowan, N.C., Gakis, G., Hernández, V.,
1602 Linares Espinós, E., Lorch, A., Neuzillet, Y., et al. (2020). European Association of Urology
1603 Guidelines on Muscle-invasive and Metastatic Bladder Cancer: Summary of the 2020
1604 Guidelines. *Eur. Urol.*
- 1605 Yanagi, K., Tanaka, T., Kato, K., Sadik, G., Morihara, T., Kudo, T., and Takeda, M. (2009).
1606 Involvement of puromycin-sensitive aminopeptidase in proteolysis of tau protein in cultured
1607 cells, and attenuated proteolysis of frontotemporal dementia and parkinsonism linked to
1608 chromosome 17 (FTDP-17) mutant tau. *Psychogeriatrics* *9*, 157–166.
- 1609 Yu, G., Wang, L.-G., Han, Y., and He, Q.-Y. (2012). clusterProfiler: an R Package for Comparing
1610 Biological Themes Among Gene Clusters. *OMICS J. Integr. Biol.* *16*, 284–287.
- 1611 (2018). Picard toolkit (Broad Institute).
- 1612